Systematic cysteine-crosslinking in native membranes establishes the transmembrane architecture in Ire1 clusters

Kristina Väth[1,2], Roberto Covino[3], John Reinhard[1,2],
Gerhard Hummer[3,4], and Robert Ernst[1,2]

[1]Medical Biochemistry and Molecular Biology, Medical Faculty, Saarland University, Kirrberger Str. 100, Building 61.4, 66421 Homburg, Germany
[2]PZMS, Center for Molecular Signaling (PZMS), Medical Faculty, Saarland University, 66421 Homburg
[3]Department of Theoretical Biophysics, Max-Planck-Institute of Biophysics, Max-von-Laue-Strasse 3, 60438 Frankfurt am Main, Germany.
[4]Institute of Biophysics, Goethe-University, 60438 Frankfurt am Main, Germany.

*To whom correspondence should be addressed
robert.ernst@uks.eu

Running title: The TMHs of signaling-active Ire1 are X-shaped

Abstract

The endoplasmic reticulum (ER) is a key organelle of membrane biogenesis and crucial for the folding of both membrane and secretory proteins. Stress sensors of the unfolded protein response (UPR) monitor the unfolded protein load in the ER and convey effector functions for the maintenance of ER homeostasis. More recently, it became clear that aberrant compositions of the ER membrane, referred to as lipid bilayer stress, are equally potent activators of the UPR with important implications in obesity and diabetes. How the distinct signals from lipid bilayer stress and proteotoxic stress are processed by the highly conserved UPR transducer Ire1 remains unknown. Here, we have generated a functional, cysteine-less variant of Ire1 and performed systematic cysteine crosslinking experiments to establish the transmembrane architecture of signaling-active clusters in native membranes. We show that the transmembrane helices of two neighboring Ire1 molecules adopt an X-shaped configuration and that this configuration is independent of the primary cause for ER stress. Based on these findings, we propose that different forms of stress converge in a single, signaling-active conformation of Ire1.

Keywords

UPR, IRE1, PERK, lipid bilayer stress, UPR-transducer, cysteine crosslinking, membrane stress, ER stress, membrane quality control

70 **Introduction**

71 The endoplasmic reticulum (ER) marks the entry-point to the secretory pathway
72 for soluble and membrane proteins. Under adverse conditions, accumulation of
73 unfolded proteins causes ER stress and initiates the unfolded protein response (UPR)
74 mediated by the Inositol-requiring enzyme 1 (Ire1) in budding yeast, and by the troika
75 of IRE1α, the PKR-like Endoplasmic Reticulum Kinase (PERK), and the activating
76 transcription factor 6 (ATF6) in vertebrates (1). Once activated, the UPR attenuates
77 the production of most proteins and initiates a wide transcriptional program to
78 upregulate ER chaperones, ER-associated degradation (ERAD), and lipid biosynthesis
79 (2). Through these mechanisms, the UPR is centrally involved in cell fate decisions
80 between life, death, and differentiation (3). Insulin-producing β-cells, for example, rely
81 on UPR signals for their differentiation into professional secretory cells, while chronic
82 ER stress caused by an excess of saturated fatty acids kills them (4). The
83 transcriptional program of the UPR controls to expression of more than five percent of
84 all genes with tremendous impact on virtually all aspects of cell physiology (2).
85 Consistent with these broad effector functions, the UPR is associated with numerous
86 diseases including diabetes, cancer, and neurodegeneration (5).

87 Ire1 is highly conserved among eukaryotes and represents the only transducer
88 of ER stress in baker's yeast (6, 7). It is a type I transmembrane protein equipped with
89 an ER-luminal sensor domain and two cytosolic effector domains: a kinase and an
90 endoribonuclease (RNase) (8–10). How exactly unfolded proteins activate the UPR via
91 direct and indirect mechanisms is a matter of active debate (11–15). ER stress caused
92 by the accumulation of unfolded proteins leads to the oligomerization of Ire1 (16),
93 which activates the cytosolic effector kinase and RNase domains (17). The
94 unconventional splicing of the *HAC1* precursor mRNA initiated by the RNase domain
95 facilitates the production of an active transcription factor that controls a broad spectrum
96 of UPR-target genes via unfolded protein response elements (UPRE) in the promotor
97 region (2, 18).

98 Lipid bilayer stress due to aberrant compositions of the ER membrane is equally
99 potent in activating the UPR (19–21). This membrane-based mechanism is conserved
100 throughout evolution (20, 22, 23) and has been implicated in the lipotoxicity associated
101 with obesity and type II diabetes (4, 24). We have shown that Ire1 from baker's yeast
102 inserts an amphipathic helix (AH) into the luminal leaflet of the ER-membrane, thereby
103 forcing the adjacent TMH in a tilted configuration that locally squeezes the bilayer (25).

104 Aberrant stiffening of the ER membrane during lipid bilayer stress would increase the
105 energetic penalty for membrane deformation and thus stabilizes an oligomeric state of
106 Ire1 via a membrane-based mechanism (25, 26).

107 The accumulation of unfolded proteins in the ER can be triggered with
108 dithiothreitol (DTT) and Tunicamycin (TM), which interfere with protein folding in the
109 ER by inhibiting disulfide bridge formation and N-linked glycosylation, respectively.
110 Lipid bilayer stress is caused, for example, by an accumulation of saturated lipids or
111 by inositol-depletion (19, 21). While both proteotoxic and membrane-based stress lead
112 to the formation of Ire1 clusters (16, 25, 27), it remains unexplored if there is only one
113 signaling-active configuration of Ire1 is or if distinct conformations trigger custom-
114 tailored responses.

115 Here, we report on a systematic dissection of Ire1's TMH region domain in
116 signaling-active clusters. We have engineered a cysteine-less variant for genomic
117 integration at the endogenous locus, generated a series of constructs featuring single
118 cysteines in the TMH region, and developed a new crosslinking approach to study the
119 transmembrane configuration of Ire1 in the natural environment of ER-derived
120 membrane vesicles featuring the native complexity of lipids and proteins. This
121 approach uncovers the transmembrane architecture of Ire1 in signaling-active clusters
122 and suggests – irrespective of the primary cause of ER-stress (i.e. unfolded proteins
123 or lipid bilayer stress) an X-shaped configuration of the TMHs from neighboring Ire1
124 molecules. Our findings underscore the crucial importance of Ire1's highly bent
125 configuration in the TMH region for stabilizing an oligomeric state via a membrane-
126 mediated mechanism.

127 **Results**

128 We employed systematic cysteine-crosslinking in the TMH region of Ire1 to gain insight
129 into the structural organization of its signaling-active clusters during ER-stress.
130 Recognizing that Ire1 is activated by aberrant physicochemical membrane properties
131 (25, 26), which are exceedingly hard to mimic using bottom-up approaches, we
132 performed these crosslinking experiments in microsomes exhibiting the natural
133 complexity of proteins and lipids of the ER membrane.

134

135 **Cysteine-less Ire1 is functional**

136 We have generated a cysteine-less version of Ire1 that would allow us to introduce
137 single cysteine residues in the TMH region for a subsequent crosslinking using copper
138 sulfate ($CuSO_4$). The cysteine-less construct is based on a previously established
139 knock-in construct of *IRE1* that provides a homogeneous, near-endogenous
140 expression level (25) and encodes for a fully-functional, epitope-tagged variant of Ire1,
141 with an 3xHA tag and monomeric, yeast-enhanced GFP (yeGFP) inserted in a flexible
142 loop at the position H875 (25, 28) (Figure 1A). To generate a cysteine-less version, we
143 have substituted each of the twelve cysteines in the luminal, transmembrane and
144 cytosolic regions of Ire1 with serine. Two cysteines in the signal sequence, which are
145 co-translationally removed, remained in the final construct to ensure correct ER-
146 targeting and membrane insertion (Figure 1A). Cysteine 48 of yeGFP ($C48^{yeGFP}$) was
147 mutated to serine, while $C70^{yeGFP}$ is present in the cysteine-less construct to ensure
148 correct folding of the fluorescent protein (29). Notably, $C70^{yeGFP}$ is buried inside the
149 fluorescent protein (30) and thus inaccessible for crosslinking agents under non-
150 denaturing conditions.

151 The steady-state level of wildtype and cysteine-less Ire1 are comparable (Figure S1A)
152 and both proteins are properly integrated into the membrane as shown by subcellular
153 fractionation (Figure S1B) and extraction assays (Figure S1C). The functionality of
154 cysteine-less Ire1 was analyzed using a sensitive assay scoring the growth of cells
155 exposed to chronic ER stress (25). Liquid cultures in minimal (synthetic complete
156 dextrose; SCD) and full (yeast peptone dextrose; YPD) media were exposed to
157 different concentrations of the reducing agent DTT and cultivated for 18 h prior to
158 determining of the optical density (OD) of the culture. Cells producing either the
159 wildtype or cysteine-less Ire1 are phenotypically indistinguishable and substantially

160 more resistant to DTT than cells lacking *IRE1* (Figure 1B). This suggests that the
161 cysteine-less variant of Ire1 is functional and capable to mount an adaptive UPR.
162 The functionality of the cysteine-less variant during ER-stress was further validated by
163 an alternative assay based on the degree of *HAC1* splicing (Figure 1C) and the mRNA
164 level of the UPR-target gene *PDI1* (Figure S1D). Exponentially growing cells were
165 acutely stressed for 1 h with either DTT or Tunicamycin, characterized by RT-qPCR,
166 and compared to unstressed cells. Expectedly, the spliced *HAC1* mRNA was
167 upregulated several-fold in stressed cells compared to unstressed cells and this
168 upregulation was observed in both wildtype and cysteine-less Ire1-producing cells.
169 (Figure 1C). Consequently, we also observed an upregulation of the mRNA of PDI1 in
170 response to ER-stress albeit to slightly lower degree for the cysteine-less version
171 compared to the wildtype construct (Figure S1D). The number of signaling-active
172 clusters per cell during ER-stress was almost identical for cells expressing either
173 wildtype and cysteine-less Ire1 (Figure S1E). We conclude that the cysteine-less
174 variant of Ire1 is functional during chronic and acute ER stress.
175
176 **Crosslinking of Ire1's TMH in ER-derived microsomes**
177 We established a strategy to crosslink a series of single-cysteine variants of clustered
178 Ire1 via copper sulfate ($CuSO_4$) in microsomes derived from the ER of stressed cells
179 (Figure 2A-C). This approach has several advantages over previous attempts and
180 provides unprecedented insights into structure-function relationships of this UPR-
181 transducer. Ire1 is studied 1) in the context of the full-length protein, 2) in ER-derived
182 microsomes featuring the native lipid environment, and 3) at a physiological protein-
183 to-lipid ratio with the full range of transmembrane proteins being present in the same
184 membrane. Using this system, we have studied the configuration of Ire1's TMH in
185 UPR-signaling clusters. Notably, these long-lived clusters are stable for several
186 minutes (16, 31). Thus, $CuSO_4$-mediated crosslinking that occurs on the same time-
187 scale can provide useful structural information even though it leads to the irreversible
188 formation of disulfide bonds under our experimental conditions.
189 Cells expressing either a cysteine-less variant of Ire1 or a variant containing a single-
190 cysteine in the TMH region (F544C) were cultivated to the mid-exponential phase in
191 minimal medium. These cells were either left untreated or stressed for 1 h with either
192 DTT (2 mM) or TM (1.5 µg/ml) to cause ER-stress, which leads to the formation of Ire1-
193 clusters (16, 25). We then isolated crude microsomes from these cells and incubated

194 them on ice for 5 min either in the presence or absence of 10 mM $CuSO_4$ to catalyze
195 the formation of disulfide bonds by oxidizing nearby sulfhydryl groups (32). Given the
196 low copy number of ~260 for Ire1 (33) and the fragmentation of the ER during
197 microsome preparation, we expect to detect crosslinking of single-cysteine variants of
198 Ire1 only when it was pre-clustered prior to the preparation.
199 Immunoblotting of the resulting samples revealed a prominent, HA-positive signal
200 corresponding to monomeric Ire1 and for some samples, a less-pronounced HA-
201 positive signal from a band with lower electrophoretic mobility that was only observed
202 when 1) Ire1 contained a single-cysteine in the TMH region (F544C), 2) the
203 microsomes were prepared from stressed cells (either DTT or TM), and 3) when
204 crosslinking was facilitated by $CuSO_4$ (Figure 2C). This suggests a remarkably specific
205 formation of covalent, disulfide bonds between two Ire1 molecules in the TMH region,
206 despite the presence of numerous other, potentially competing membrane proteins
207 with exposed cysteines in the ER. A Co-IP analysis using Flag-tagged and HA-tagged
208 Ire1 variants co-produced in a single cell and crosslinked in microsomes via the native
209 cysteine in the TMH region (C552) verified that the additional band with low
210 electrophoretic mobility represented presumably disulfide-linked, SDS-resistant dimers
211 of Ire1 (Figure S2). We conclude that Ire1 variants with single cysteines in the TMH
212 region can be specifically cross-linked via $CuSO_4$, when present as pre-formed clusters
213 in microsomes isolated from stressed cells.
214
215 **A crosslinking screen identifies an X-shaped configuration of Ire1's TMH**
216 Next, we systematically introduced single cysteine-residues in the TMH-region of Ire1
217 in order to characterize the structural configuration of Ire1's TMH in signaling-active
218 clusters. We generated a total of thirteen variants each containing a single cysteine in
219 the TMH region starting with E540C at the transition between the AH and the TMH
220 (Figure 3A) and ending at the residue C552, a native TMH residue that is substituted
221 to serine in the cysteine-less Ire1. Consequently, this scanning approach covered more
222 than three helical turns and almost the entire short TMH of Ire1 (Figure 3A, B). All
223 variants with engineered cysteine residues (E540C to F551C) were subjected to a
224 sensitive, cell-based assay to ascertain the functionality of the UPR under condition of
225 prolonged ER stress (Figure S3A). Consistent with the functional role of the AH in the
226 ER-luminal membrane leaflet (25), we found that the substitution of an AH-residue to
227 cysteine (E540C, T541C, or G542C) impaired the stress response of Ire1 as evident

228 from the increased sensitivity of the respective cells (Figure S3A). Notably, this
229 increased sensitivity to DTT is indeed due to a functional defect because the mutations
230 do not alter the steady-state level of the Ire1 variants (Figure S2B). In contrast,
231 substitution of TMH residues (V543C-F551C) did not result in an impaired resistance
232 to DTT in the respective cells (Figure S3A). This suggests that these TMH residues
233 have no specific relevance for Ire1 activation (Figure S3A). We then subjected this set
234 of single cysteine variants to the established cysteine-crosslinking procedure (Figure
235 3C). While some variants (e.g. G542C or L546C) showed no detectable crosslinking,
236 a significant portion of other variants (e.g. T541C or L549C) was crosslinked under the
237 given experimental conditions (Figure 3C,D). The F544C variant consistently exhibited
238 the highest crosslinking efficiency (Figure 3C,D). The overall pattern of crosslinking
239 residues in the TMH residues was independent of the condition of ER stress
240 (Figure 3D). Proteotoxic stress induced by either DTT, TM or lipid bilayer stress caused
241 by inositol-depletion (19, 34) showed essentially the same crosslinking pattern
242 (Figure S3C, 3D). These data suggest that the structural organization of Ire1 in
243 signaling-active clusters is comparable for different types of stress, at least in the TMH
244 region.
245 Cysteine crosslinking can be used to infer structural models. The observed pattern of
246 crosslinking residues in the TMH of Ire1 is very distinct to those observed in the TMH
247 region of the growth hormone receptor (35) and the thrombopoietin receptor (36),
248 which form parallel dimers leading to a helical periodicity of crosslinking. Our data also
249 disfavor a model of the two TMHs - attached to the ER-luminal and cytosolic portions
250 of Ire1 via flexible loops – forming dynamic complexes in an entirely random
251 orientation. Instead, our crosslinking data suggest an X-shaped configuration of the
252 TMHs with the best-crosslinking residue F554 positioned at the crossing point.
253 Intriguingly, such an arrangement would be consistent with the previously reported,
254 highly tilted orientation of the monomeric TMH of Ire1, which is enforced by the
255 adjacent, ER-luminal AH (25).
256 In order to obtain a structural representation of these crosslinking data, we modeled a
257 dimer of the TMH region of Ire1 based on extensive molecular dynamics (MD)
258 simulations in lipid membranes that integrated the crosslinking data, and in particular
259 the contact between the two F544 (Figure 4, Supplementary Movie) and restrained the
260 two F544 residues to face each other. The resulting model of the TMH region
261 highlighted the overall, highly bent architecture of the TMH region of each protomer

262 leading to an X-shaped configuration of the dimer (Figure 4, Supplementary Movie).
263 Substantial membrane thinning and water penetration, which were previously
264 observed around the monomeric TMH region of Ire1 (25), become clearly apparent
265 and are most significant in the region of the AHs (Figure S4, Supplementary Movie).
266
267 **Validating the structural model of the TMH region of Ire1**
268 Our crosslinking approach has identified the TMH residue F544 as a candidate residue
269 that might stabilize the transmembrane configuration of Ire1 in signaling-active
270 clusters. Interestingly, an aromatic residue in the TMH region of the mammalian IRE1α
271 (W547) was reported to stabilize the oligomeric state of IRE1α (37). Hence, we
272 embarked on testing a similar role for F544 in Ire1 from baker's yeast. We generated
273 a F544A mutation, which contained the native C552 in the TMH. A cell-based assay
274 revealed that the F544A mutant was phenotypically indistinguishable from cysteine-
275 less Ire1 (Figure 5A) just as the F544C mutant (Figure S1A), thereby suggesting that
276 F544 is not functionally relevant. This finding was corroborated by Cu^{2+}-mediated
277 crosslinking of C552 in microsomes isolated from cells stressed either with DTT or TM.
278 The intensity of the band corresponding to crosslinked Ire1 was unaffected by the
279 F544A mutation (Figure 5B). Thus, F544 does not contribute to the stability of Ire1-
280 oligomers even though it is placed in close proximity to equivalent residues on the TMH
281 of neighboring Ire1 molecules.
282 Our structural model of the monomeric TMH (25) and the dimeric TMH
283 (Figure 4, Supplementary Movie) suggested an unusual, tilted architecture of the TMH
284 region, which is stabilized by the ER-luminal AH. We proposed that this configuration
285 of the TMH region facilitates Ire1 to sense aberrant membrane properties by
286 contributing to the stability of oligomeric Ire1 during lipid bilayer stress (25, 38). We put
287 this model to the test, by combining the single-cysteine F544C for crosslinking with the
288 AH-disruption F531R mutation. The resulting F531R/F544C double mutant exhibited
289 only a very mild functional defect as implied by the cellular resistance to prolonged
290 stress caused by DTT (Figure 5C). Strikingly, the disruption of the AH by the F531R
291 mutation greatly impaired the crosslinking propensity of the F544C thereby suggesting
292 an important contribution of the AH to the transmembrane architecture of Ire1
293 (Figure 5D). An analogous set of experiments was performed with a construct that
294 contained an AH-disrupting F531R mutation (25) and, as a single cysteine the native
295 TMH residue C552. This F531R/C552 construct was functionally impaired

296 (Figure S5A) and showed a significantly reduced crosslinking propensity compared to
297 the equivalent construct with an intact AH (Figure S5B), thereby highlighting structural
298 and functional importance of the ER-luminal AH.
299
300 **Discussion**
301 Here, we establish a structural model for the TMH region of Ire1 in signaling-active
302 clusters (Figure 4). Employing a systematic cysteine crosslinking approach in native
303 membranes and aided by molecular dynamics simulations, we show that neighboring
304 TMHs of clustered Ire1 are organized in an X-shaped configuration during ER-stress.
305 Based on the remarkable similarity of the crosslinking patterns observed in the context
306 of lipid bilayer stress caused by inositol-depletion and proteotoxic stress caused by
307 DTT or TM (Figure 3, Figure S3C), we propose that different forms of ER-stress
308 converge in a single, signaling-active configuration in the TMH region. Our structural
309 and functional analyses reveal a crucial role of the transmembrane architecture in
310 controlling the oligomeric state of Ire1. The finding that the F544A mutation of the best-
311 crosslinking residue at the intersection of neighboring TMHs causes no functional
312 defect (Figure 5A,B) reinforces our interpretation that Ire1 senses lipid bilayer stress
313 via its unusual architecture rather than by stereospecific, structural elements in the
314 TMH.
315 Our findings are consistent with a crucial role of the ER-luminal AH in forcing
316 the adjacent TMH in a highly tilted and bent configuration and deforming the membrane
317 (25) (Figure 4, Figure S4, Supplementary Video). We show that disrupting the
318 functionally important AH by incorporation of a charged residue into the hydrophobic
319 face substantially reduces the crosslinking efficiency, thereby implying a significant
320 structural change (Figure 5C,D and Figure S5A,B).
321 Modeling the dimeric transmembrane organization aided by the crosslinking
322 data provides intriguing insights into membrane-deforming potential of Ire1 (Figure, 4,
323 Figure S4, Supplementary Video). The ER-luminal AH and a cluster of charged
324 residues at the cytosolic end of the TMH locally distort the bilayer, which is best
325 evidenced by a decreased membrane thickness in the proximity of the monomeric (25)
326 and dimeric transmembrane domain of Ire1 (Supplementary Video). Such membrane
327 deformations also cause disordering of lipid acyl chains and come at an energetic cost,
328 which is controlled by the composition and physical properties of the surrounding
329 bilayer (38, 39). The higher this cost e.g. due to increased lipid saturation or inositol-

330 depletion, the higher is the energetic gain upon coalescing these regions and thus the
331 propensity of Ire1 to oligomerize.

332 This membrane-based activation of the UPR is not restricted to yeast, but has
333 also been reported for UPR transducers in worms (23, 40), fishes (41), and mammals
334 (20, 37, 42). In fact, all three transducers of the UPR from mammals can be activated
335 by aberrant membrane signals albeit via distinct mechanisms (20, 37, 43). The IRE1α-
336 and PERK-dependent branches of the UPR respond to increased lipid saturation even
337 when the ER-luminal domain is removed (20). While some studies suggested that
338 stress-sensing relies on generic features in the TMH of mammalian IRE1α, which are
339 independent of the exact amino acid sequence in the TMH region (20, 44), a more
340 recent study proposed a mechanism of sensing that is based on specific residues in
341 the TMH (37). Cho *et al*. scored the oligomerization propensity of IRE1α in cells via
342 bimolecular fluorescence complementation in palmitate-treated cells and suggested
343 that the increased lipid saturation might induce a conformational switch in the TMH
344 region, which relies on a tryptophan (W457) as putative sensing residue and a
345 conserved leucine zipper motif (SxxLxxx) involving serine 450 (37, 44). Intriguingly,
346 such a rotation-based mechanism of sensing would be reminiscent of the lipid
347 saturation sensor Mga2 from baker's yeast controlling the expression of the essential
348 fatty acid desaturase-encoding gene *OLE1* (45, 46).

349 We propose that Ire1 from baker's yeast uses a mechanism distinct from that
350 proposed for mammalian IRE1α based on the following evidence: 1) Mutagenesis in
351 the entire TMH of Ire1 from baker's yeast causes no functional defect unless the
352 integrity of the AH is disrupted (25). 2) Mutagenesis of individual TMH residues (V543-
353 F551) including three aromatic residues lining one side of the TMH – one of which
354 being the best-crosslinking residue F544C - causes no relevant functional defects
355 (Figure S3A). These findings are notable because aromatic residues have been
356 implicated in lipid/membrane sensing in other systems (37, 45, 46). 3) Our crosslinking
357 data provide no evidence for a rotational re-organization of the TMHs during lipid
358 bilayer stress (Figure 3C,D, Figure S3C). 4) Our cell-based assays and crosslinking
359 data underscore the central importance of an intact AH adjacent to the TMH for normal
360 UPR activity and crosslinking in the TMH region.

361 Based on similar physicochemical features of the TMH region including the
362 evolutionary conserved AH, we propose that the mammalian PERK might use a similar
363 mechanism as Ire1 from baker's yeast, while the mammalian IRE1α -as a variation to

364 a common theme- seems to employ a distinct mechanism (37, 44). Clearly, more
365 studies with an increased temporal and spatial resolution that do not interfere with the
366 dynamic properties of Ire1 will be required to identify the unique specializations of
367 individual UPR transducers and to unequivocally establish their structural and dynamic
368 features that govern their membrane sensitivity.

369 Our combined results lead to the following model. The activity of Ire1 requires
370 an oligomerization of its cytosolic effector domains, which mediate the splicing of the
371 *HAC1* in yeast of *XBP1* in mammals for signal propagation (1). This oligomerization
372 involves the entire protein as a response to divergent activating signals, which are
373 sensed by different portions of the protein.

374 Unfolded proteins are sensed by the ER-luminal domain via a binding groove (12),
375 which is formed by two interacting ER-luminal domains and is further facilitated by a
376 subsequent formation of higher oligomers (47). Under these conditions, the
377 transmembrane domain and the cytosolic effector domains 'follow' the oligomerization
378 of the ER-luminal domains. A large diversity of ER-luminal and cytosolic interactors
379 including chaperones can tune and specify the activity of mammalian UPR transducers
380 (14, 48). This may reflect a way to custom-tailor the globally-acting UPR to different
381 cell types with distinct protein folding requirements during steady-state and particularly
382 during differentiation. Lipid bilayer stress activates the UPR in both yeast and
383 mammals via a membrane-based mechanism and does not require the binding of
384 unfolded proteins to the ER-luminal domain and/or associated chaperones (19, 20,
385 25).

386 We propose that prolonged and chronic forms of ER-stress, which can be
387 mimicked by sub-lethal doses of DTT or TM, activate the UPR predominantly via this
388 membrane-based mechanism. When Ire1 is rendered insensitive to proteotoxic stress
389 by mutations in the binding groove for unfolded proteins (19, 25) and even when the
390 entire ER-luminal domain of IRE1α was substituted by a zipper domain (49) the
391 resulting proteins are activated under these conditions. We suggest that all portions of
392 Ire1, the ER-luminal domain, the TMD and the cytosolic domains cooperate in
393 determining the stability of oligomeric configurations of Ire1. An intriguing implication
394 of this model is that different forms of ER-stress would be independent of each other,
395 but inter-dependent in a somewhat additive fashion. Lipid bilayer stress would sensitize
396 Ire1 to unfolded proteins and, conversely, an increased load of unfolded proteins in the
397 ER lumen would increase the sensitivity of Ire1 to aberrant lipid compositions (20, 38).

398 The intriguing hypothesis that chemically distinct signals from the lumen and the
399 membrane of the ER cooperate in UPR activation remains to be experimentally tested.
400 Clearly, more studies are required to better understand the molecular
401 mechanisms of signal integration by UPR transducers particularly in the context of
402 prolonged and chronic ER stress. The clinical relevance is obvious as ER-stress and
403 UPR activation have been implicated the inflammatory response (50), B-cell
404 differentiation into plasma cells (51), insulin resistance, and pancreatic β-cell failure
405 (4). It has been speculated that the sensing of lipid bilayer stress by IRE1α and PERK
406 might account for instances, where relatively modest levels of unfolded protein load
407 lead to substantial UPR signaling and has been termed anticipatory UPR (52). An
408 exciting alternative possibility is that the membrane-based UPR may be caused by an
409 overcrowding of the ER membrane with membrane proteins (38, 53).
410 We have established a cysteine-less, functional variant of Ire1 allowing for a
411 detailed structure-function analysis of this UPR transducer in its native membrane
412 context. This construct and the established protocol for cysteine-crosslinking can be
413 readily adapted to address other central questions regarding the structural organization
414 of signaling-active clusters of Ire1, which may be inaccessible by other approaches.
415

416 **Materials and Methods**

417

418 **Reagents and Antibodies**

419 All chemicals and reagents used in this study were purchased from Sigma
420 Aldrich, Carl Roth or Millipore and are of analytical or higher grade. The following
421 antibodies were used: mouse anti-Flag monoclonal (M2) (Santa Cruz), rat anti-HA
422 monoclonal (3F19) (Roche), mouse anti-Dpm1 monoclonal (5C5A7) (Life
423 Technologies), mouse anti-Pgk1 (22C5D8) (Life Technologies), mouse anti-MBP
424 monoclonal (NEB), anti-mouse-HRP (Dianova), anti-rat-HRP (Dianova).

425

426 **Strains and plasmids**

427 All strains used in this study are listed in Table 1, plasmids are listed in Table 2.

428

429 **Genetic manipulation of *S. cerevisiae***

430 For genetic manipulation of *S. cerevisiae*, we used a previously described
431 knock-in strategy (25). This construct comprised the endogenous promoter of *IRE1* (−1
432 to −551 bp), the sequence of *IRE1* with a sequence coding for a 3xHA tag and a
433 monomeric version of yeGFP (A206R ^{yeGFP}) inserted at the position of H875, and the
434 endogenous 5′ terminator sequence on the plasmid pcDNA3.1-IRE13xHA-GFP (25).
435 A cysteine-less variant of this construct was generated by substituting all 12 cysteines
436 in *IRE1* with serine using a strategy based on the QuikChange method (Stratagene).
437 Additionally, the cysteine 48 (C48 ^{yeGFP}) of the monomeric yeGFP was substituted to
438 serine, while the inaccessible, functionally relevant cysteine 70 (C70 ^{yeGFP}) remained
439 in the final construct (29, 30). Derivatives of this constructs were generated by
440 substituting individual codons of TMH residues to cysteine. All mutants used in this
441 study are listed in Table 2. These plasmids were linearized using Hind*III* and Xho*I*
442 restriction enzymes and used for transforming a previously established cloning strain
443 lacking both the gene of IRE1 and its promotor (25). Strains used in this study are
444 listed in Table 1.

445 Additionally, a Flag-tagged cysteine-less Ire1 version based on the CEN-based
446 Ire1 construct from the pPW1628/pEv200 plasmid (28) was generated. The 3xHA
447 epitope tag in the knock-in construct was replaced by a 3xFlag epitope tag using the
448 Q5 site-directed mutagenesis kit (NEB). The newly generated knock in sequence was
449 amplified in a multi-step PCR reaction adding the terminator sequence from the

450 pEv200 plasmid and *BssH*I and *Hind*III restriction site. The transfer of the *IRE1*$_{3xFlag\text{-}GFP}$
451 sequence in the *CEN*-based vector pPW1628/pEv200 (28) was performed using
452 *BssH*I/*Hind*III restriction sites.
453
454 **Cultivation of *S. cerevisiae***
455 The yeast strains were cultivated at 30°C on agar plates containing SCD
456 complete medium or selection medium. Liquid yeast cultures were inoculated with a
457 single colony and typically cultivated at 30°C for a minimum of 18 h to reach the
458 stationary phase. This overnight culture was used to inoculate a fresh culture, which
459 was inoculated to an OD_{600} = 0.2 and cultivated until the mid-exponential cultures.
460 For microsomal membrane preparation, stationary cells were used to inoculate
461 a fresh culture in SCD complete medium to an OD_{600} of 0.2. After cultivation at 30°C
462 to an OD_{600} of 0.7, the cells were either left untreated or stressed with either 2 mM DTT
463 or 1.5 µg/ml Tunicamycin for 1 h. For inositol depletion, exponentially growing cells
464 were washed with inositol-depleted media and used to inoculate the main culture to an
465 OD_{600} of 0.5 in SCD complete w/o inositol, which was further cultivated for 3 h.
466
467 **Live cell confocal microscopy**
468 A fresh culture in SCD medium was inoculated to an OD_{600} = 0.2 and cultivated
469 for 5.5 h. To induce ER-stress, DTT was added to a final concentration of 2 mM
470 followed by additional cultivation for 1 h. The cells were harvested placed on
471 microscopic slides coated with a thin layer of SCD containing 1.5% agarose for
472 immobilization. Microscopy was performed using a Zeiss LSM 780 confocal laser
473 scanning microscope (Carl Zeiss AG) with spectral detection and a Plan-Apochromat
474 63x 1.40 NA oil immersion objective. GFP fluorescence was excited at 488 nm and the
475 emission was detected between 493 and 598 nm. Transmission images were
476 simultaneously recorded using differential interference contrast (DIC) optics. Z-stacks
477 (450 nm step-size, 62.1 µm pinhole size) were recorded. Ire1-clusters were identified
478 by automated segmentation using CellProfiler (54). In brief, cellular areas of the field
479 of view were determined based on sum projections of recorded z-stacks. Clusters
480 within these cells were identified by adaptive thresholding of the respective maximum
481 intensity z-projections.
482
483

484 **Preparation of cell lysates and immunoblotting**

485 Lysates were prepared from exponentially growing cells, which were harvested
486 by centrifugation (3.000xg, 5 min, 4°C) and then washed once with ddH_2O and once
487 with PBS. During washing, the cells were transferred into 1.5 ml reaction tubes allowing
488 for a more rapid centrifugation (8.000xg, 20 sec, 4°C). The tubes with the washed cell
489 pellet were placed in a -80°C freezer and stored until further use.

490 For preparing a cell lysate, either 5 or 20 OD equivalents were resuspended in
491 400 µl or 1000 µl lysis buffer (PBS containing 30 µg/ml protease inhibitor cocktail),
492 respectively. After addition of either 100 µl or 500 µl of zirconia beads, respectively,
493 the cells were disrupted by bead beating for 5 min at 4°C. Four volumes units of the
494 resulting lysate were mixed with one volume of 5x reducing sample buffer (8M urea,
495 0.1 M Tris-HCl pH 6.8, 5 mM EDTA, 3.2% (w/v) SDS, 0.15% (w/v) bromphenol blue,
496 4% (v/v) glycerol, 4% (v/v) β-mercaptoethanol) and then incubated at 95°C for 10 min
497 for fully unfolding and solubilizing the proteins therein. 0.1 OD equivalents of the
498 resulting sample was subjected to SDS-PAGE and the proteins were separated on
499 4-15% Mini-PROTEAN-TGX strain-free gels (BioRad). For subsequent immuno-
500 blotting, proteins were transferred from the gel to methanol-activated PVDF
501 membranes using semi-dry Western-Blotting. Specific proteins were detected using
502 antigen-specific primary antibodies, HRP-coupled secondary antibodies, and
503 chemiluminescence.

504

505 **Assaying the resistance to ER-stress**

506 Stationary overnight cultures were used to inoculate a fresh culture to an OD_{600}
507 of 0.2. After cultivation for 5 to 7 h at 30°C the cells were diluted with pre-warmed
508 medium to an OD_{600} of 0.05. 50 µl of these diluted cultures were mixed in a 96-well
509 plate with 180 µl of medium and 20 µl of a DTT dilution series leading to a final
510 concentration of DTT between 0 and 2 mM and 0 and 4 mM, respectively. After
511 incubation at 30°C for 18 h, the cultures were thoroughly mixed and 200 µl of the cell
512 suspension were transferred to a fresh 96-well plate for determining the density of the
513 culture via a photospectrometer using the OD_{600}/OD_{620}.

514

515

516

517 **RNA preparation, cDNA synthesis and quantitative real-time (qPCR) PCR**
518 **analysis**
519 Exponentially growing cells were used to inoculate a 20 ml culture to an OD_{600}
520 of 0.2 in YPD. After cultivation for 3 h, the cells were either left untreated or stressed
521 with either 4 mM DTT or 1.0 µg/ml Tunicamycin. After an additional cultivation for 1 h,
522 5 OD equivalents were harvested by centrifugation (3.000xg, 5 min, RT). The
523 supernatant was discarded while the pellet was snap frozen in liquid N_2 and stored at
524 -80°C. The RNA was prepared from these cells using the RNeasy Plus RNA Isolation
525 Kit (Qiagen). 500 ng RNA of the total isolated RNA were used as a template for the
526 synthesis of cDNA using Oligo(dT) primers and the Superscript™ II RT protocol
527 (Invitrogen). qPCR was performed using ORA qPCR Green ROX L Mix (HighQu) in a
528 Piko Real PCR system (Thermo Scientific). The following primers were used to amplify
529 DNA sequences of interest:
530 *HAC1s* forward primer: 5' – CTTTGTCGCCCAAGAGTATGCG – 3'
531 *HAC1s* reverse primer: 5' – ACTGCGCTTCTGGATTACGC – 3'
532 *ACT1* forward primer: 5' – TGTCACCAACTGGGACGATA – 3'
533 *ACT1* reverse primer: 5' – AACCAGCGTAAATTGGAACG – 3'
534 All reactions were performed in technical duplicates. Non-template controls (RNA) and
535 non-reaction controls (H_2O) were additionally performed. The qPCR program included
536 the following steps: 1) 95°C, 15 min; 2) 95°C, 20 sec; 3) 58°C, 20 sec; 4) 72°C, 30 sec;
537 5) 72°C, 5 min; steps 2-4 were repeated 40 times. The relative quantification of *HAC1*
538 splicing levels was based on the comparative ΔΔCT method using normalization to
539 *ACT1* levels (StepOnePlus™ user Manual, Applied Biosystems).
540
541 **Microsomal membrane preparation**
542 80 OD_{600} equivalents were harvested from a mid-exponential culture by
543 centrifugation (3.000xg, 5 min, 4°C), washed with PBS, and stored at -80°C. All steps
544 of membrane fractionation were performed on ice or at 4°C with pre-chilled buffers.
545 The cell pellets were resuspended in 1.5 ml lysis buffer (50 mM HEPES pH 7.0, 150
546 mM NaCl, 1 mM EDTA, 10 µg/ml chymostatin, 10 µg/ml antipain, 10 µg/ml pepstatin).
547 For cysteine crosslinking experiments, a lysis buffer without EDTA was used. Cells
548 were disrupted by using zirconia beads (Roth) and a bead beater (2 x 5 min). Cell
549 debris was removed from the lysate by centrifugation (800x g, 5 min, 4°C) and further
550 cleared from major mitochondrial contaminations (5,000 x g, 10 min, 4°C). The pellet

551 was discarded, and the supernatant was spun again (100.000x g, 45 min, 4°C) to
552 obtain a crude microsomal fraction in the pellet. The microsomes were resuspended
553 in 1.4 ml lysis buffer, sonicated for homogenization (50%, 5x1sec, MS72 tip on a
554 sonifier cell disrupter from Branson Ultrasonic) snap frozen in liquid N_2 in small aliquots
555 to avoid freeze-thaw cycles, and stored at -80°C for further use.
556
557 **Test of membrane association**
558 The cleared supernatant of a 5.000xg step was divided into equal parts, which
559 were then mixed with an equal volume of lysis buffer supplemented with 0.2 M Na_2CO_3
560 resulting in a final pH of 11, 5 M urea, 2% Triton X-100 or without additional additives.
561 After incubation for 1 h on a rotator, these samples were centrifuged (100,000x g, 45
562 min, 4°C) to separate soluble from insoluble material. The supernatant and pellets from
563 these fractions corresponding to 0.2 OD equivalents were further analyzed by SDS-
564 PAGE and immunoblotting.
565
566 **$CuSO_4$-induced cysteine crosslinking**
567 For cysteine crosslinking with $CuSO_4$, the microsomes were thawed on ice. 8 µl
568 of microsomes with a protein concentration of 1 ± 0.2 mg/ml were then incubated with
569 2 µl of 50 mM $CuSO_4$ in ddH_2O resulting in a final concentration of 10 mM $CuSO_4$ and
570 incubated for 5 min. A sample supplemented with 2 µl ddH_2O served as a non-
571 crosslinking control. The reaction was stopped with 8 µl of membrane sample buffer
572 (4 M urea, 50 mM Tris-HCl pH 6.8, 1.6 % (w/v) SDS, 0.01% (w/v) bromophenol blue,
573 2% (v/v) glycerol) including 125 mM EDTA and 250 mM NEM. Samples were heated
574 for 5 min at 95°C and further analyzed by SDS-PAGE and immunoblotting. The
575 percentage of dimer formation was determined using the densiometric signals of the
576 bands corresponding to the monomeric and covalently dimeric protein, which were
577 determined using ImageJ.
578
579 **Immunoprecipitation from microsomes after $CuSO_4$-induced cysteine**
580 **crosslinking**
581 300 µl of microsomes with a typical protein concentration of 1 mg/ml were
582 incubated with 12.5 µl 250 mM $CuSO_4$ (final concentration of 10 mM) for 5 min on ice.
583 The reaction was stopped by adjusting the sample to a final concentration of 50 mM
584 EDTA and 111 mM NEM by adding 30 µl of 0.5 M EDTA stock solution and 44 µl of 1

585 M NEM stock solution, respectively. The final volume was adjusted to 1.3 ml with lysis
586 buffer with a final concentration of 5 mM EDTA. The $CuSO_4$ concentration was thus
587 reduced to 2.4 mM and the NEM concentration to 33.6 mM, respectively.
588 After crosslinking, the microsomes were solubilized using 2% Triton X-100 and
589 incubated for 1 h at 4°C under constant agitation. Insoluble material was removed by
590 centrifugation (20.000x g, 10 min, 4°C). The resulting supernatant was incubated with
591 8 µl Flag beads (Sigma Aldrich), equilibrated with IP wash buffer (lysis buffer + 5 mM
592 EDTA + 0.2 % Triton X-100), for 3 h under constant shaking. Flag beads were washed
593 five times with IP wash buffer by centrifugation (8.000xg, 30 sec, 4°C). For elution, the
594 Flag beads were incubated with 10 µl IP-Wash and 10 µl 5x reducing sample buffer
595 for 5 min at 95°C, which did not disrupt the disulfide bond formed between to protomers
596 of Ire1. These samples were analyzed by SDS-PAGE and immunoblotting.
597
598 **Modelling of the dimer**
599 We extracted an equilibrated conformation of a monomeric 56 amino-acid long
600 sequence 516-SRELD EKNQNSLLLK FGSLVYRIIE TGVFLLLFLI FCAILQRFKI
601 LPPLYVLLSK I-571 from a previously performed 10 µs long equilibrium MD simulation.
602 We duplicated the configuration in order to create a new system containing two
603 identical protomers. We then rotated and translated one of the two protomers to form
604 a dimer structure, such that the two F544 faced each other with the distance between
605 their Cβ atoms at around 0.7 nm. A short energy minimization in solution resolved all
606 steric clashes between side-chains. The structure of the model dimer was prepared by
607 using gromacs/2019.3 tools (55) and VMD (56). We used Charmm-GUI (57, 58) to
608 reconstitute the dimer in a bilayer containing 248 POPC and 62 cholesterol molecules
609 modelled in the Charmm36m force-field (59–61). We solvated the system with 24813
610 TIP3P water molecules, 72 chloride and 66 sodium ions, corresponding to a salt
611 concentration of 150 mM.
612
613 **Equilibrium and restrained simulations of the dimer model**
614 After an initial energy minimization and quick relaxation, we carefully
615 equilibrated the dimer model in the bilayer. We first ran a 50 ns long simulation
616 restraining the position of protein atoms by using harmonic potentials with force-
617 constants (in units of kJ mol^{-1} nm^2) of 500 for backbone atoms and 200 for side-chain
618 atoms. We then ran further 50 ns lowering the force-constants to 200 and 50,

619 respectively. After this equilibration, we relieved all restraints and ran two independent
620 500 ns long MD simulations. In the first simulation, the system evolved according to its
621 unbiased dynamics; in the second, we restrained the distance between the two Cβ
622 atoms of F544 on each protomer, gradually driving them closer in time. We first
623 centered the restraining harmonic potential around 0.5 nm with a force-constants (in
624 units of kJ mol^{-1} nm^2) of 1000. We then lowered the equilibrium distance of the potential
625 and decreased the force-constants (in units of kJ mol^{-1} nm^2): 0.4 nm and 750 after
626 10 ns from the beginning of the run; 0.3 nm and 500 after 20 ns; and 0.2 nm and 500
627 after 30 ns and for the remaining duration of the simulation.
628 We ran both the restrained equilibration and unbiased production simulation in
629 gromacs/2019.3, and the restrained production simulation in gromacs/2018.7 patched
630 with the open-source, community-developed PLUMED library (62) version 2.5 (63),
631 using a time step of 2 fs. Electrostatic interactions were evaluated with the Particle-
632 Mesh-Ewald method (64). We maintained a constant temperature of 303 K (65),
633 applying separate thermostats on the protein, membrane, and solvent with a
634 characteristic time of 1 ps. We applied the semi-isotropic Berendsden barostat (66) for
635 the restrained equilibration, and the Parrinello-Rahman barostat (67) for the production
636 runs, acting separately on the x-y plane and z direction to maintain a constant pressure
637 of 1 atm, and with a characteristic time of 5 ps. We constrained all hydrogen bonds
638 with the LINCS algorithm (68). Molecular visualizations were obtained with VMD and
639 rendered with Tachyon.
640
641 **Data analysis, representation, and statistical tests**
642 The amount of crosslinked dimer was determined using the densiometric signals of the
643 bands corresponding to the monomeric and covalently dimeric protein. The percentage
644 was calculated from the ratio of dimer signal to whole Ire1 signal. The software Image
645 J was used for the determination if the densiometric signal.
646 Throughout the manuscript, the data are represented as the average ± SEM. All
647 experiments were performed at least in triplicates. The significance was tested by
648 unpaired Student's t tests. Further information regarding statistical analysis can be
649 found in the figure legends. In the following, the exact value of n is provided for every
650 dataset of this paper.

651 **Fig. 1B**: left panel: Δ*IRE1*, WT: n=21 (technical replicates from four individual
652 colonies); cysteine-less: n=12 (technical replicates from four individual
653 colonies)
654 right panel: Δ*IRE1*: n=15 (technical replicates from three individual
655 colonies); cysteine-less: n=12 (technical triplicates from four individual
656 colonies); WT: n=9 (technical triplicates from three individual colonies)
657 **Fig. 1C**: left panel: WT -DTT: n= 4; WT +DTT: n=6; cysteine-less -DTT: n=6;
658 cysteine-less +DTT: n=5
659 Right panel: WT -TM: n=4; WT +TM: n=5; cysteine-less -TM: n=6; cysteine-
660 less +TM: n=4
661 **Fig. 3D**: DTT: E540C, T541C: n=8 (technical duplicates from four individual
662 colonies); G542C, V543C, L545C, L546C, L547C, F548C, L549C, I550C,
663 F551C: n=4 (technical duplicates from two individual colonies); F544C:
664 n=14 (technical duplicates from seven individual colonies); C552: n=11
665 (technical duplicates from six individual colonies)
666 TM: E540C, T541C: n=8 (technical duplicates from four individual colonies);
667 G542C, V543C, L545C, L546C, L547C, F548C, L549C, I550C, F551C: n=4
668 (technical duplicates from two individual colonies); F544C: n=10 (technical
669 duplicates from five individual colonies); C552: n=8 (technical duplicates
670 from four individual colonies)
671 Inositol depletion: n=6 (technical duplicates from three individual colonies)
672 **Fig. 5A:** Δ*IRE1*, cysteine-less: n=12 (technical replicates from two individual
673 colonies), F544A C552: n=12 (technical triplicates from four individual
674 colonies)
675 **Fig. 5B**: DTT: C552: n=11 (technical duplicates from six individual colonies), F544A
676 C552: n=4 (technical duplicates from two individual colonies)
677 TM: C552: n=8 (technical duplicates from four individual colonies), F544A
678 C552: n=4 (technical duplicates from two individual colonies)
679 **Fig. 5C:** Δ*IRE1*, cysteine-less: n=12 (technical replicates from two individual
680 colonies), F531R F544C: n=12 (technical triplicates from four individual
681 colonies)
682 **Fig. 5D**: DTT: F544C: n=14 (technical duplicates from seven individual colonies),
683 F531R F544C: n=4 (technical duplicates from two individual colonies)

684 TM: F544C n=10 (technical duplicates from five individual colonies), F531R
685 F544C: n=4 (technical duplicates from two individual colonies)
686 **Fig. S1B**: left panel: WT -DTT: n= 5; WT +DTT: n=5; cysteine-less -DTT: n=6; cysteine-
687 less +DTT: n=6
688 Right panel: WT -TM: n=5; WT +TM: n=5; cysteine-less -TM: n=6; cysteine-
689 less +TM: n=3
690 **Fig. S3A**: OD_{620}: Δ*IRE1*: n=9 (technical triplicates from three individual colonies):
691 cysteine-less: n=12 (technical triplicates from four individual colonies);
692 E540C – L546C: n=6 (technical triplicates from two individual colonies)
693 OD_{600}: ΔIRE1: n=10 (technical replicates from three individual colonies):
694 cysteine-less: n=22 (technical triplicates from four individual colonies);
695 L547C – F551: n=6 (technical triplicates from two individual colonies)
696 **Fig. S4A**: Δ*IRE1*, cysteine-less: n=12 (technical replicates from two individual
697 colonies), F544R C552: n=9 (technical triplicates from three individual
698 colonies)
699 **Fig. S5B**: DTT: C552: n=11 (technical duplicates from six individual colonies), F531R
700 C552: n=4 (technical duplicates from two individual colonies)
701 TM: C552: n=8 (technical duplicates from four individual colonies), F531R
702 C552: n=4 (technical duplicates from two individual colonies
703

704 **References**

705 1. Walter P, Ron D (2011) The unfolded protein response: from stress pathway to
706 homeostatic regulation. *Science* 334(6059):1081–1086.
707 2. Travers KJ, et al. (2000) Functional and genomic analyses reveal an essential
708 coordination between the unfolded protein response and ER-associated
709 degradation. *Cell* 101(3):249–258.
710 3. Hetz C (2012) The unfolded protein response: Controlling cell fate decisions
711 under ER stress and beyond. *Nat Rev Mol Cell Biol* 13(2):89–102.
712 4. Fonseca SG, Burcin M, Gromada J, Urano F (2009) Endoplasmic reticulum
713 stress in β-cells and development of diabetes. *Curr Opin Pharmacol* 9(6):763–
714 770.
715 5. Kaufman RJ (2002) Orchestrating the unfolded protein response in health and
716 disease. *J Clin Invest* 110(10):1389–1398.
717 6. Nikawa J, Yamashita S (1992) IRE1 encodes a putative protein kinase
718 containing a membrane-spanning domain and is required for inositol
719 phototrophy in Saccharomyces cerevisiae. *Mol Microbiol* 6(11):1441–1446.
720 7. Kimata Y, Kohno K (2011) Endoplasmic reticulum stress-sensing mechanisms
721 in yeast and mammalian cells. *Curr Opin Cell Biol* 23(2):135–142.
722 8. Cox JS, Shamu CE, Walter P (1993) Transcriptional induction of genes
723 encoding endoplasmic reticulum resident proteins requires a transmembrane
724 protein kinase. *Cell* 73(6):1197–1206.
725 9. Sidrauski C, Walter P (1997) The transmembrane kinase Ire1p is a site-specific
726 endonuclease that initiates mRNA splicing in the unfolded protein response.
727 *Cell* 90(6):1031–1039.
728 10. Mori K, Ma W, Gething MJ, Sambrook J (1993) A transmembrane protein with
729 a cdc2+/CDC28-related kinase activity is required for signaling from the ER to
730 the nucleus. *Cell* 74(4):743–756.
731 11. Karagöz GE, et al. (2017) An unfolded protein-induced conformational switch
732 activates mammalian IRE1. *Elife* 6:e30700.
733 12. Gardner BM, Walter P (2011) Unfolded proteins are Ire1-activating ligands that
734 directly induce the unfolded protein response. *Science* 333(6051):1891–1894.
735 13. Adams CJ, Kopp MC, Larburu N, Nowak PR, Ali MMU (2019) Structure and
736 Molecular Mechanism of ER Stress Signaling by the Unfolded Protein
737 Response Signal Activator IRE1. *Front Mol Biosci* 6:11.

738 14. Amin-Wetzel N, et al. (2017) A J-Protein Co-chaperone Recruits BiP to
739 Monomerize IRE1 and Repress the Unfolded Protein Response. *Cell*
740 171(7):1625-1637.e13.
741 15. Bertolotti A, Zhang Y, Hendershot LM, Harding HP, Ron D (2000) Dynamic
742 interaction of BiP and ER stress transducers in the unfolded-protein response.
743 *Nat Cell Biol* 2(6):326–332.
744 16. Kimata Y, et al. (2007) Two regulatory steps of ER-stress sensor Ire1 involving
745 its cluster formation and interaction with unfolded proteins. *J Cell Biol*
746 179(1):75–86.
747 17. Korennykh A V, et al. (2009) The unfolded protein response signals through
748 high-order assembly of Ire1. *Nature* 457(7230):687–93.
749 18. Mori K, et al. (1992) A 22 bp cis-acting element is necessary and sufficient for
750 the induction of the yeast KAR2 (BiP) gene by unfolded proteins. *EMBO J*
751 11(7):2583–2593.
752 19. Promlek T, et al. (2011) Membrane aberrancy and unfolded proteins activate
753 the endoplasmic reticulum stress sensor Ire1 in different ways. *Mol Biol Cell*
754 22(18):3520–3532.
755 20. Volmer R, van der Ploeg K, Ron D (2013) Membrane lipid saturation activates
756 endoplasmic reticulum unfolded protein response transducers through their
757 transmembrane domains. *Proc Natl Acad Sci U S A* 110(12):4628–4633.
758 21. Surma MA, et al. (2013) A lipid E-MAP identifies Ubx2 as a critical regulator of
759 lipid saturation and lipid bilayer stress. *Mol Cell* 51(4):519–530.
760 22. Ho N, Xu C, Thibault G (2018) From the unfolded protein response to
761 metabolic diseases – lipids under the spotlight. *J Cell Sci* 131(3):jcs199307.
762 23. Hou NS, et al. (2014) Activation of the endoplasmic reticulum unfolded protein
763 response by lipid disequilibrium without disturbed proteostasis in vivo. *Proc*
764 *Natl Acad Sci U S A* 111(22):E2271-2280.
765 24. Pineau L, Ferreira T (2010) Lipid-induced ER stress in yeast and β cells:
766 Parallel trails to a common fate. *FEMS Yeast Res* 10(8):1035–1045.
767 25. Halbleib K, et al. (2017) Activation of the Unfolded Protein Response by Lipid
768 Bilayer Stress. *Mol Cell* 67(4):673-684.e8.
769 26. Ernst R, Ballweg S, Levental I (2018) Cellular mechanisms of physicochemical
770 membrane homeostasis. *Curr Opin Cell Biol* 53:44–51.
771 27. Li H, Korennykh A V, Behrman SL, Walter P (2010) Mammalian endoplasmic

772 reticulum stress sensor IRE1 signals by dynamic clustering. *Proc Natl Acad Sci*
773 *U S A* 107(37):16113–16118.
774 28. van Anken E, et al. (2014) Specificity in endoplasmic reticulum-stress signaling
775 in yeast entails a step-wise engagement of HAC1 mRNA to clusters of the
776 stress sensor Ire1. *Elife* 3:e05031.
777 29. Costantini LM, et al. (2015) A palette of fluorescent proteins optimized for
778 diverse cellular environments. *Nat Commun* 6(1):7670.
779 30. Orm M, et al. (1996) Crystal Structure of the Aequorea victoria Green
780 Fluorescent Protein. *Science (80-)* 273(5280):1392–1395.
781 31. Cohen N, et al. (2017) Iron affects Ire1 clustering propensity and the amplitude
782 of endoplasmic reticulum stress signaling. *J Cell Sci* 130(19):3222–3233.
783 32. Kobashi K (1968) Catalytic oxidation of sulfhydryl groups by o-phenanthroline
784 copper complex. *BBA - Gen Subj* 158(2):239–245.
785 33. Ghaemmaghami S, et al. (2003) Global analysis of protein expression in yeast.
786 *Nature* 425(6959):737–741.
787 34. Lajoie P, Moir RD, Willis IM, Snapp EL (2012) Kar2p availability defines distinct
788 forms of endoplasmic reticulum stress in living cells. *Mol Biol Cell* 23(5):955–
789 64.
790 35. Brooks AJ, et al. (2014) Mechanism of Activation of Protein Kinase JAK2 by
791 the Growth Hormone Receptor. *Science (80-)* 344(6185):1249783–1249783.
792 36. Matthews EE, et al. (2011) Thrombopoietin receptor activation: transmembrane
793 helix dimerization, rotation, and allosteric modulation. *FASEB J* 25(7):2234–
794 2244.
795 37. Cho H, et al. (2019) Intrinsic Structural Features of the Human IRE1α
796 Transmembrane Domain Sense Membrane Lipid Saturation. *Cell Rep*
797 27(1):307-320.e5.
798 38. Covino R, Hummer G, Ernst R (2018) Integrated Functions of Membrane
799 Property Sensors and a Hidden Side of the Unfolded Protein Response. *Mol*
800 *Cell* 71(3):458–467.
801 39. Radanović T, Reinhard J, Ballweg S, Pesek K, Ernst R (2018) An emerging
802 group of membrane property sensors controls the physical state of organellar
803 membranes to maintain their identity. *BioEssays* 40(5):e1700250.
804 40. Koh JH, Wang L, Beaudoin-Chabot C, Thibault G (2018) Lipid bilayer stress-
805 activated IRE-1 modulates autophagy during endoplasmic reticulum stress. *J*

806 *Cell Sci* 131(22):jcs217992.
807 41. Thakur PC, Davison JM, Stuckenholz C, Lu L, Bahary N (2014) Dysregulated
808 phosphatidylinositol signaling promotes endoplasmic-reticulum-stress-
809 mediated intestinal mucosal injury and inflammation in zebrafish. *Dis Model*
810 *Mech* 7(1):93–106.
811 42. Kitai Y, et al. (2013) Membrane lipid saturation activates IRE1α without
812 inducing clustering. *Genes to Cells* 18(9):798–809.
813 43. Tam AB, et al. (2018) The UPR Activator ATF6 Responds to Proteotoxic and
814 Lipotoxic Stress by Distinct Mechanisms. *Dev Cell* 46(3):327-343.e7.
815 44. Kono N, Amin-Wetzel N, Ron D (2017) Generic membrane-spanning features
816 endow IRE1α with responsiveness to membrane aberrancy. *Mol Biol Cell*
817 28(17):2318–2332.
818 45. Covino R, et al. (2016) A eukaryotic sensor for membrane lipid saturation. *Mol*
819 *Cell* 63(1):49–59.
820 46. Ballweg S, Sezgin E, Wunnicke D, Haenelt I, Ernst R (2019) Regulation of lipid
821 saturation without sensing membrane fluidity.
822 doi:https://doi.org/10.1101/706556.
823 47. Korennykh A, Walter P (2012) Structural Basis of the Unfolded Protein
824 Response. *Annu Rev Cell Dev Biol* 28(1):251–77.
825 48. Sepulveda D, et al. (2018) Interactome Screening Identifies the ER Luminal
826 Chaperone Hsp47 as a Regulator of the Unfolded Protein Response
827 Transducer IRE1α. *Mol Cell* 69(2):238-251.e8.
828 49. Liu CY, Schroder M, Kaufman RJ (2000) Ligand-independent dimerization
829 activates the stress response kinases IRE1 and PERK in the lumen of the
830 endoplasmic reticulum. *J Biol Chem* 275(32):24881–24885.
831 50. Zhang K, Kaufman RJ (2008) From endoplasmic-reticulum stress to the
832 inflammatory response. *Nature* 454(7203):455–462.
833 51. Hu CCA, Dougan SK, McGehee AM, Love JC, Ploegh HL (2009) XBP-1
834 regulates signal transduction, transcription factors and bone marrow
835 colonization in B cells. *EMBO J* 28(11):1624–1636.
836 52. Rutkowski DT, Hegde RS (2010) Regulation of basal cellular physiology by the
837 homeostatic unfolded protein response. *J Cell Biol* 189(5):783–794.
838 53. Michell RH (2018) Do inositol supplements enhance phosphatidylinositol
839 supply and thus support endoplasmic reticulum function? *Br J Nutr* 120(3):301–

840 316.
841 54. McQuin C, et al. (2018) CellProfiler 3.0: Next-generation image processing for
842 biology. *PLoS Biol* 16(7):e2005970.
843 55. Abraham MJ, et al. (2015) Gromacs: High performance molecular simulations
844 through multi-level parallelism from laptops to supercomputers. *SoftwareX* 1–
845 2:19–25.
846 56. Humphrey W, Dalke A, Schulten K (1996) VMD: Visual molecular dynamics. *J*
847 *Mol Graph* 14(1):33–38.
848 57. Wu EL, et al. (2014) CHARMM-GUI membrane builder toward realistic
849 biological membrane simulations. *J Comput Chem* 35(27):1997–2004.
850 58. Lee J, et al. (2016) CHARMM-GUI Input Generator for NAMD, GROMACS,
851 AMBER, OpenMM, and CHARMM/OpenMM Simulations Using the
852 CHARMM36 Additive Force Field. *J Chem Theory Comput* 12(1):405–413.
853 59. Klauda JB, et al. (2010) Update of the CHARMM All-Atom Additive Force Field
854 for Lipids: Validation on Six Lipid Types. *J Phys Chem B* 114(23):7830–7843.
855 60. Best RB, et al. (2012) Optimization of the additive CHARMM all-atom protein
856 force field targeting improved sampling of the backbone φ, ψ and side-chain
857 χ(1) and χ(2) dihedral angles. *J Chem Theory Comput* 8(9):3257–3273.
858 61. Huang J, et al. (2016) CHARMM36m: An improved force field for folded and
859 intrinsically disordered proteins. *Nat Methods* 14(1):71–73.
860 62. PLUMED consortium (2019) Promoting transparency and reproducibility in
861 enhanced molecular simulations. *Nat Methods* 16(8):670–673.
862 63. Tribello GA, Bonomi M, Branduardi D, Camilloni C, Bussi G (2014) PLUMED 2:
863 New feathers for an old bird. *Comput Phys Commun* 185(2):604–613.
864 64. Essmann U, et al. (1995) A smooth particle mesh Ewald method. *J Chem Phys*
865 103(19):8577–8593.
866 65. Bussi G, Donadio D, Parrinello M (2007) Canonical sampling through velocity
867 rescaling. *J Chem Phys* 126(1):014101.
868 66. Berendsen HJC, Postma JPM, Van Gunsteren WF, Dinola A, Haak JR (1984)
869 Molecular dynamics with coupling to an external bath. *J Chem Phys*
870 81(8):3684–3690.
871 67. Parrinello M, Rahman A (1981) Polymorphic transitions in single crystals: A
872 new molecular dynamics method. *J Appl Phys* 52(12):7182–7190.
873 68. Hess B, Bekker H, Berendsen HJC, Fraaije JGEM (1998) LINCS: A Linear

Constraint Solver for molecular simulations. *J Comput Chem* 18(12):1463–1472.

Acknowledgements

This work was supported by the Deutsche Forschungsgemeinschaft (SFB807 'Transport and Communication across Biological Membranes' to R.E. and G.H.; SFB894 'Ca^{2+}-Signals: Molecular Mechanisms and Integrative Functions' to R.E). R.C. and G.H. were supported by the Max Planck Society. We thank Carsten Mattes for excellent technical support and especially Kristina Halbleib for her important contributions during the early phase of the project.

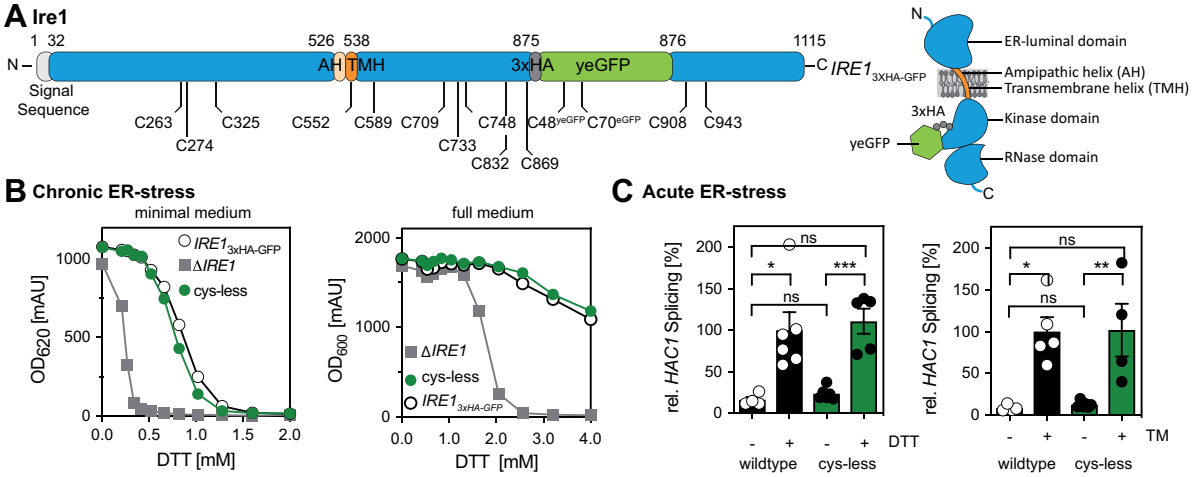

Fig. 1: Cysteine-less Ire1 expressed from its endogenous locus is functional. (*A*) Schematic representations of the knock-in construct *IRE1*$_{3xHA\text{-}GFP}$ indicating the position of cysteine residues and topology. All twelve cysteines of Ire1 and C48 ^{yeGFP} of yeGFP were substituted to serine to generate a cysteine-less variant. Cysteine 70 of yeGFP (C70 ^{yeGFP}) is functionally relevant (29) and remained in the final construct. The two cysteines in the signal sequence of Ire1 have not been replaced, as the signal sequence is removed upon ER-translocation. (*B*) Resistance of the indicated yeast strains to chronic ER-stress. Stationary overnight cultures of the indicated yeast strains were used to inoculate a fresh culture in full or minimal media to an OD_{600} of 0.2. After cultivation for 5 to 7 h at 30°C the cells were diluted with pre-warmed full or minimal media to an OD_{600} of 0.1. Cells were cultivated for 18 h at 30°C in the indicated media and stressed with DTT. The density of the resulting culture was determined using the OD_{620} or OD_{600}. (*C*) Relative levels of spliced *HAC1* mRNA in acutely stressed cells normalized to the degree of *HAC1* slicing in stressed cells expressing *IRE1*$_{3xHA\text{-}GFP}$ wildtype. Exponentially growing cells of the indicated strains were used to inoculated fresh YPD media to an OD_{600} of 0.2, cultivated in YPD and acutely stressed with either 4 mM DTT (left panel) or 1.0 µg/ml Tunicamycin (right panel) for 1 h. The relative level of spliced *HAC1* in these cells was analyzed by RT-qPCR and quantitated using the comparative ΔΔCT method using normalization to *ACT1* levels. The data were normalized to the splicing of *HAC1* in stressed cells carrying the *IRE1*$_{3xHA\text{-}GFP}$ wildtype construct. All error bars in this figure represent the mean ± SEM of at least three independent experiments. Significance was tested by an unpaired, two-tailed Student's t test. ***p<0.001, **p<0.01, *p<0.05.

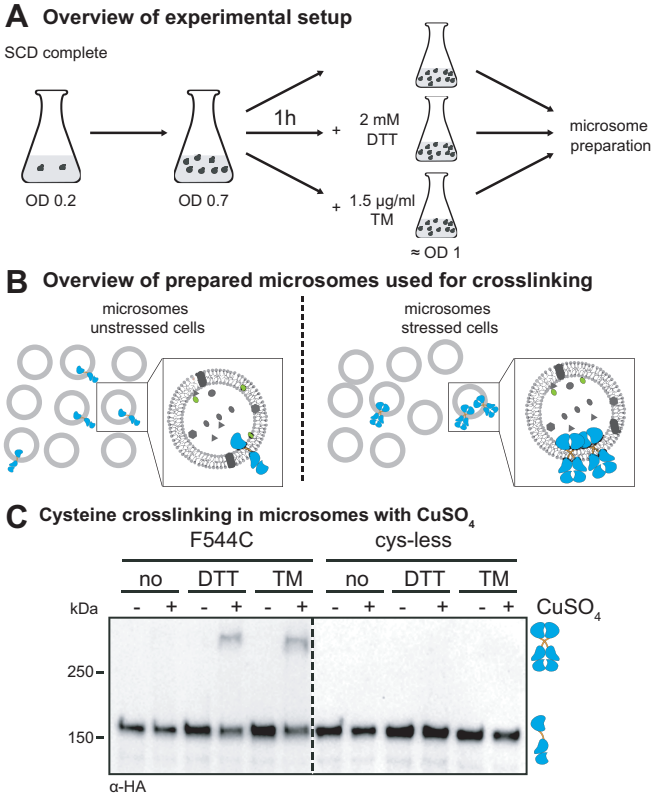

Fig. 2: The crosslinking of Ire1 via single cysteines in microsomes requires $CuSO_4$ and pre-formed clusters. (*A*) Overview of the cultivation of yeast cells for cysteine crosslinking. Stationary cells were used to inoculate a fresh culture in SCD complete media to an OD_{600} of 0.2. After cultivation at 30°C to an OD_{600} of 0.7, Ire1-clustering was induced either by DTT (1h, 2 mM, SCD) or TM (1h, 1.5 µg/ml, SCD). After harvesting the unstressed and stressed cells, cells were lysed and used for microsomal membrane preparation by differential centrifugation. (*B*) Overview of cysteine crosslinking with $CuSO_4$. Microsomes from unstressed cells and microsomes from stressed cells containing Ire1 clusters were incubated with $CuSO_4$ to induce cysteine crosslinking of Ire1. (*C*) Crosslinking of single cysteine variants of Ire1 in microsomes. The indicated strains were cultivated in the presence and absence of ER-stressors. Cells were cultivated and treated as described in (*A*). 80 OD equivalents of cells were harvested and disrupted prior to the preparation of crude microsomes by differential centrifugation. The crosslinking of juxta-posed cysteines was induced by 10 mM $CuSO_4$ on ice and an incubation for 5 min. 8 µl microsomes with a typical protein concentration of 1 mg/ml were incubated with 2 µl 50 mM $CuSO_4$. The reaction was stopped by the addition of 2 µl 1 M NEM, 2 µl 0.5 M EDTA and 4 µl membrane sample buffer. The resulting samples were subjected to SDS-PAGE corresponding to 0.25 OD equivalents and analyzed by immunoblotting using a monoclonal anti-HA antibody.

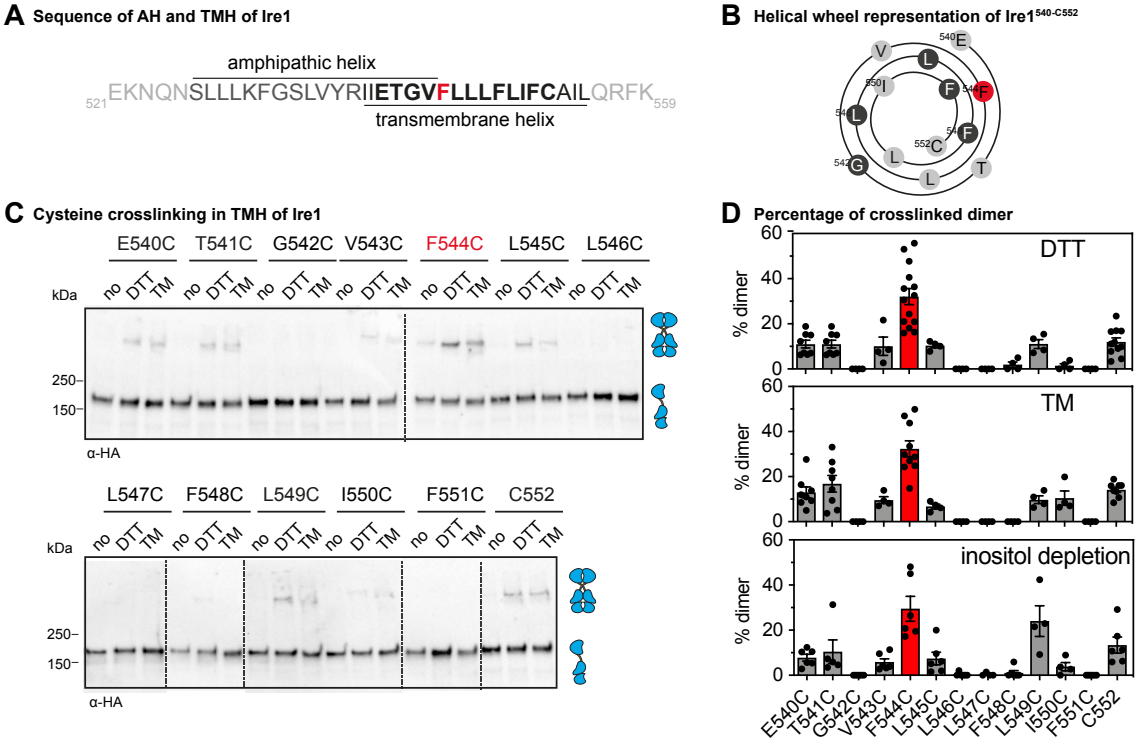

Figure 3: Systematic crosslinking of cysteines in the TMH region of Ire1 reveals a specific configuration during ER stress. (*A*) Primary structure of TMH region of Ire1 including the adjacent ER-luminal amphipathic helix (25). Almost all residues of the short TMH (shown in bold) were systematically mutated to cysteines for $CuSO_4$ crosslinking and are illustrated as helical wheel representation in (*B*). (*B*) Helical wheel representation of the TMH residues ($Ire1^{540-552}$) subjected to the cysteine scanning approach. (*C*) Crosslinking of single cysteine variants of Ire1 in microsomes. Stationary cells were used to inoculate fresh SCD complete media to an OD_{600} of 0.2. After cultivation to an OD_{600} of 0.7 at 30°C, cells were treated either with 2 mM DTT or 1.5 µg/ml TM in SCD medium for 1 h. Microsomes from unstressed cells (no) and stressed cells were prepared by differential centrifugation and subjected to a $CuSO_4$-mediated crosslinking procedure. 8 µl microsomes were incubated with 2 µl 50 mM $CuSO_4$ (final concentration 10 mM) for 5 min on ice. After the reaction was stopped with NEM, EDTA and membrane sample buffer, the samples (0.25 OD equivalents) were subjected to SDS-PAGE followed by immunoblotting using anti-HA antibodies. (*D*) Quantification of tested UPR stress conditions. Cells were cultivated and treated as described in (*C*). For inositol depletion, exponentially growing cells were inoculated to an OD_{600} of 0.5 and cultivated for 3h in inositol depleted media. Cells were harvested and treated as described in (*C*). Immunoblots of crosslinked microsomes from cells depleted from inositol are shown in Fig. S3. The percentage of crosslinked dimer from at least three independent experiments was determined using the densiometric signals of the bands illustrated in (*C*) (ER stressors: DTT and TM) and Fig S3. (ER stressors: inositol depletion) corresponding to the monomeric and covalently dimeric protein, which were determined using ImageJ (n > 4, mean ± SEM).

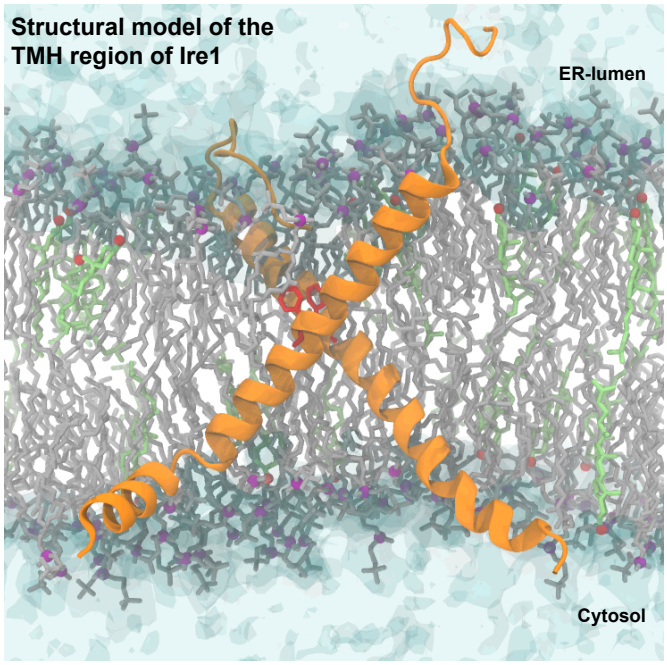

Figure 4: Structural model of the TMH region of Ire1.
Configuration of a model TMH dimer obtained from atomistic molecular dynamics simulations. Protomers are shown as an orange ribbon, with the residues F544 highlighted in red. POPC lipids and their phosphate moiety are shown in gray and purple, respectively. Cholesterol molecules and their hydroxyl groups are shown in light green and red, respectively. Water is shown in a transparent surface representation.

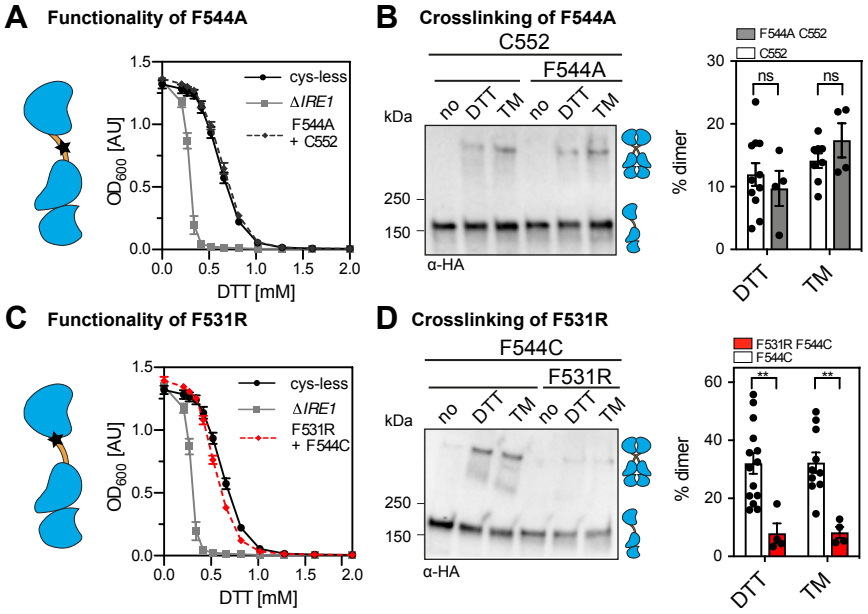

Figure 5: The impact of mutations in the TMH and the AH of Ire1 on its functionality and crosslinking propensity. (*A*) The ER-stress resistance of cells expressing the F544A variant of $Ire1_{3xHA\text{-}GFP}$ containing the native cysteine 552 was scored using a yeast growth assay. Stationary overnight cultures of the indicated yeast strains were used to inoculate a fresh culture to an OD_{600} of 0.2. After cultivation for 5 to 7 h at 30°C, the cells were diluted with fresh media to an OD_{600} of 0.1. Cells were cultivated for 18 h at 30°C in the presence of the indicated concentrations of DTT. The density of the resulting culture was determined using the OD_{600}. (*B*) The impact of the F544A mutation in the TMH of Ire1 on the degree of crosslinking via cysteine 552 was determined using the microsome-based crosslinking assay. Stationary cultures were used to inoculate fresh SCD complete media to an OD_{600} of 0.2 and cultivated to an OD_{600} of 0.7. Cells were stressed by the addition of 2 mM DTT or 1.5 µg/ml TM for 1 h. Microsomes of 80 OD units of the indicated yeast strains were prepared by differential centrifugation and used for cysteine crosslinks. 8 µl microsomal membranes were incubated with 2 µl $CuSO_4$ (final concentration 10 mM) and incubated for 5 min on ice. The reaction was stopped by adding 8 µl stopping buffer. Samples corresponding to 0.25 OD equivalents were subjected to SDS PAGE and a subsequent immunoblotting with anti-HA antibodies. (*C*) The ER-stress resistance of cells expressing the AH-disrupting F531R variant of $Ire1_{3xHA\text{-}GFP}$ containing the native cysteine 552 was scored using a yeast growth assay. The indicated cells were cultivated and treated as in (*A*). (*D*) The impact of the AH-disrupting F531R mutation of Ire1 on the degree of crosslinking via cysteine 552 was determined using the microsome-based crosslinking assay. Cells were cultivated and further treated as described in (*B*). The data are represented as the mean ± SEM and are derived from at least three independent experiments. Significance was tested by an unpaired, two-tailed Student's t test. **p<0.01.

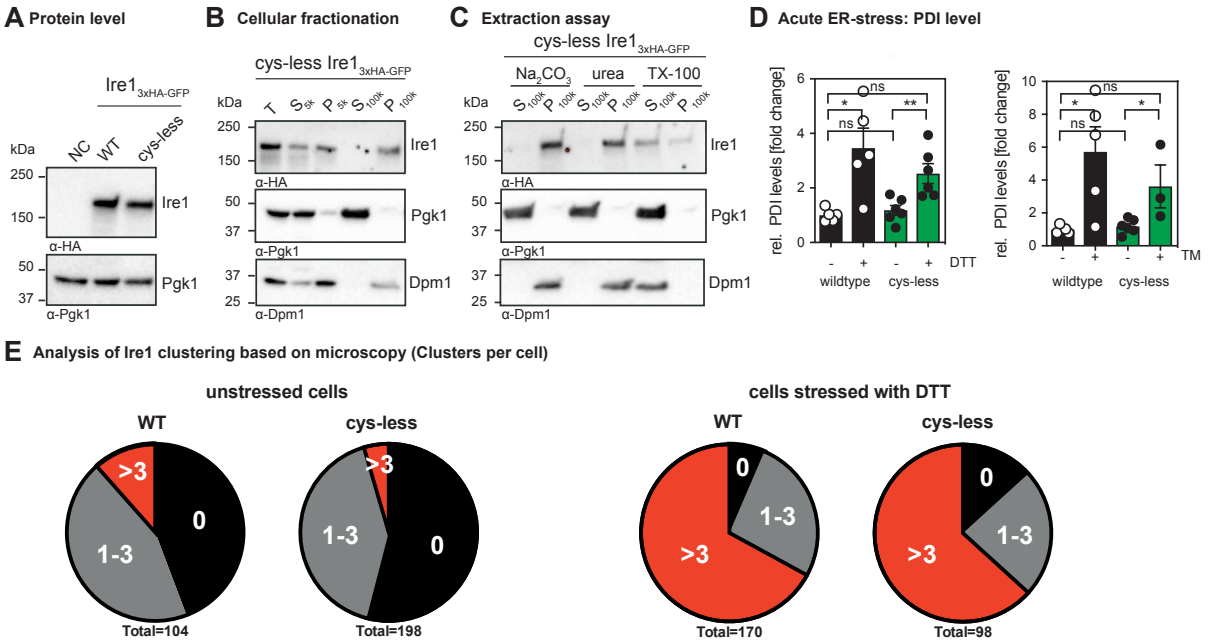

Fig. S1: Protein levels of cysteine-less Ire1 and characterization of its membrane association. (*A*) Protein levels of cells expressing either *IRE1*$_{3xHA\text{-}GFP}$ WT or the cysteine-less (cysteine-less) variant. The isogenic wildtype strain BY4741 that does not express a HA-tagged variant of IRE1 was used as a specificity control (NC). Stationary overnight cultures were used to inoculate a fresh culture in SCD complete to an OD_{600} of 0.2 and cultivated until an OD_{600} of 1 was reached. 0.1 OD equivalents of cell lysates were immunoblotted using anti-HA and anti-Pgk1 antibodies. (*B*) Subcellular fractionation of exponentially growing cells expressing cysteine-less *IRE1*$_{3xHA\text{-}GFP}$ by differential centrifugation at 5,000 x g and 100,000 x g. Stationary overnight cultures were used to inoculate a fresh culture in SCD complete to an OD_{600} of 0.2 and cultivated until an OD_{600} of 1 was reached. 80 OD_{600} equivalents were harvested and used for microsomal membrane preparation. The individual supernatant and pellet fractions were analyzed by immunoblotting using anti-HA, anti-Pgk1 and anti-Dpm1 antibodies by loading 0.4 OD equivalents. (*C*) Extraction assay of microsomes. Carbonate and urea extraction validate proper membrane integration of cysteine-less *IRE1*$_{3xHA\text{-}GFP}$ (cysteine-less). Samples of each step corresponding to 0.2 OD equivalents were analyzed by immunoblotting using anti-HA, anti-Pgk1 and anti-Dpm1 antibodies. (*D*) PDI levels in acutely stressed cells normalized to the fold change of unstressed cells expressing *IRE1*$_{3xHA\text{-}GFP}$ wildtype. Exponentially growing cells of the indicated strains were used to inoculated fresh YPD media to an OD_{600} of 0.2, cultivated in YPD and acutely stressed with either 4 mM DTT (left panel) or 1.0 µg/ml Tunicamycin (right panel) for 1 h. The relative level of *PDI* in these cells was analyzed by RT-qPCR and quantitated using the comparative ΔΔCT method using normalization to *ACT1* levels. The data were normalized to the *PDI* level in unstressed cells carrying the *IRE1*$_{3xHA\text{-}GFP}$ wildtype construct. All error bars in this figure represent the mean ± SEM of at least three independent experiments. Significance was tested by an unpaired, two-tailed Student's t test. **p<0.01, *p<0.05. (E) Analysis of fluorescent clusters by microscopy in the indicated cells expressing either *IRE1*$_{3xHA\text{-}GFP}$ WT or the cysteine-less construct. The number of clusters per cell was determined for the indicated conditions and plotted in the pie chart. The total number of analyzed cells is given for each condition.

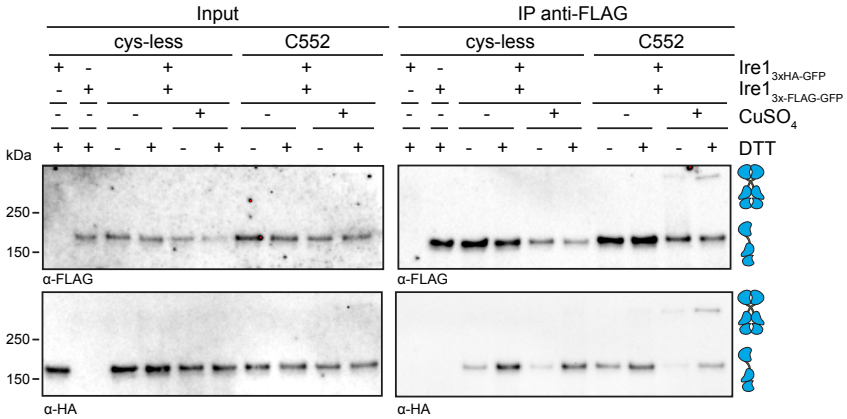

Fig. S2. Co-immunoprecipitation validates the formation of homo-dimers of Ire1 in crosslinking experiments. A crosslinking experiment using $CuSO_4$ was performed with microsomes prepared from cells expressing a HA-tagged variant of Ire1 from endogenous locus (*IRE1*$_{3xHA\text{-}GFP}$) and a Flag-tagged variant (*IRE1*$_{3xFlag\text{-}GFP}$) from a *CEN*-based plasmid. A yeast culture in selective SCD-LEU was inoculated to an OD_{600} of 0.2 from a stationary overnight culture and cultivated at 30°C until an OD_{600} of 0.7 was reached. The cells were either stressed with 2 mM DTT or left untreated and were further cultivated for 1 h. 80 OD_{600} equivalents from these cultures were harvested by centrifugation. Microsomal membranes were isolated by differential centrifugation. Microsomes prepared from cells expressing only one of the two tagged variants of Ire1 served as controls. Both constructs contained a single cysteine in the TMH region at the position 552 (C552). After incubation of the microsomes with 10 mM $CuSO_4$ on ice for 5 min, the crosslinking reaction was stopped by the addition of NEM in a final concentration of 111 mM and EDTA in a final concentration of 50 mM. The microsomes were then solubilized using 2% Triton X-100 and subjected to an IP using anti-Flag beads. Both the input and IP samples were analyzed by immunoblotting using anti-Flag and anti-HA antibodies.

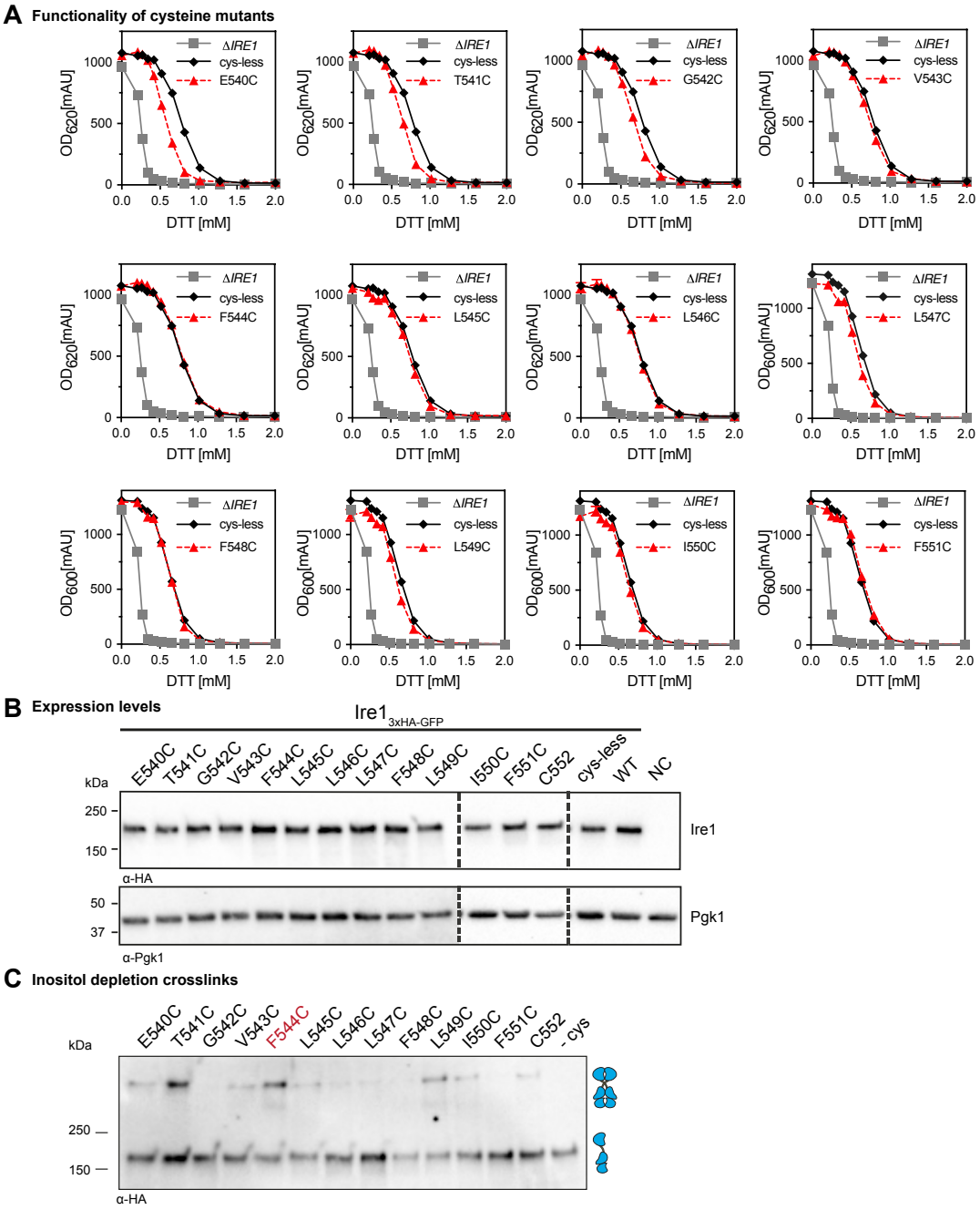

Figure S3: Functionality of cysteine mutants and their crosslinking potential in lipid bilayer stress conditions. (*A*) The resistance to ER-stress was investigated for the indicated yeast strains. Stationary overnight cultures of the indicated yeast strains were used to inoculate a fresh culture in full or minimal media to an OD_{600} of 0.2. After cultivation for 5 to 7 h at 30°C the cells were diluted with fresh minimal media to an OD_{600} of 0.1. Cells were cultivated for 18 h at 30°C and stressed with DTT. The density of the resulting culture was determined using the OD_{620} or OD_{600}. The error bars represent the mean ± SEM of at least two independent clones. (*B*) Protein levels of cells expressing different *IRE1*$_{3xHA\text{-}GFP}$ variants. The lysates of exponentially growing cells were immunoblotted using anti-HA and anti-Pgk1 antibodies. (*C*) Crosslinking of single cysteine variants of Ire1 in microsomes derived from cells grown in lipid bilayer stress conditions. Exponentially growing cells in SCD complete media were washed and used to inoculate a fresh media w/o inositol to an OD_{600} of 0.5. To induce lipid bilayer stress, the cells were grown in inositol depleted SCD complete media for 3 h. 80 OD equivalents were harvested and used for microsomal membrane preparation.

1061 $CuSO_4$ induced crosslink was performed by incubating 8 µl of microsomes with 2 µl of
1062 50 mM $CuSO_4$ for 5 min on ice. After stopping the reaction with NEM and EDTA,
1063 samples were subjected to SDS-PAGE with a subsequent immunoblotting with anti-
1064 HA antibody.
1065

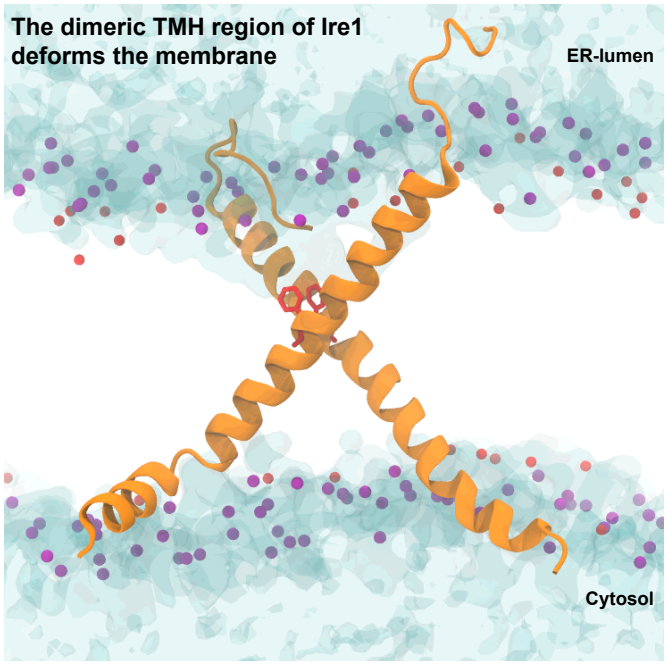

Figure S4: The dimeric TMH region of Ire1 deforms the membrane.
Configuration of a model TMH dimer obtained from atomistic molecular dynamics simulations. Protomers are shown as an orange ribbon, with the residues F544 highlighted in red. The phosphate moieties of POPC are shown as purple beads. Rhe hydroxyl groups of cholesterol molecules are shown as red beads. Water is shown in a transparent surface representation.

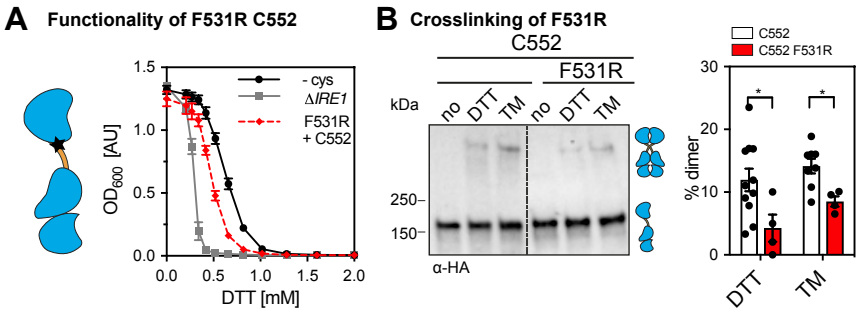

Fig. S5: The impact of the AH mutation of Ire1 on its functionality and crosslinking propensity. (*A*) The ER-stress resistance of cells expressing the F544A variant of $Ire1_{3xHA\text{-}GFP}$ containing the native cysteine 552 was scored using the yeast growth assay as described in Figure 5. (*B*) The impact of the F544A mutation in the TMH of Ire1 on the degree of crosslinking via cysteine 552 was determined using the microsome-based crosslinking assay. The data are represented as the mean ± SEM and are derived from at least three independent experiments. Significance was tested by an unpaired, two-tailed Student's t test. *p<0.05.

1085 **Supplementary Movie: A structural model of the TMH region of Ire1 highlights**
1086 **membrane thinning and water penetration into the bilayer.**

1087 **Table 1: Yeast strains of used in this study**

Strain No,	Description	Genotype	Source
RE001	BY4741	BY4741 MATa; *his*3Δ1; *leu2*Δ0; *met15*Δ0; *ura3*Δ0	Euroscarf
RE046	Δ*IRE1*	BY4741 MATa; *his3*Δ1; *leu2*Δ0; *met15*Δ0; ura3Δ0; *ire1*Δ::kanMX4	Euroscarf
RE127	Δ*IRE1*Δ*IRE1promotor*	BY4741 MATa; *his3*Δ1; *leu2*Δ0; *met15*Δ0; *ura3*Δ0; *ire1*Δ::URA pUG72	(25)
RE425	*IRE1*-3xHA-yeGFP	BY4741 MATa; *his3*Δ1; *leu2*Δ0; *met15*Δ0; *ura3*Δ0; *ire1*Δ::URA *IRE1*-3xHA-yeGFP::HIS pRE451	(25)
RE343	*IRE1*-3xHA-yeGFP *cysteine-less*	BY4741 MATa; *his3*Δ1; *leu2*Δ0; *met15*Δ0; *ura3*Δ0; *ire1*Δ::URA *IRE1*-3xHA-yeGFP::HIS pRE375	This paper
RE342	*IRE1*-3xHA-yeGFP C552	BY4741 MATa; *his3*Δ1; *leu2*Δ0; *met15*Δ0; *ura3*Δ0; *ire1*Δ::URA *IRE1*-3xHA-yeGFP::HIS pRE374	This paper
RE725	*IRE1*-3xHA-yeGFP cysteine-less + CEN IRE1-3xFLAG-yeGFP *cysteine-less*	BY4741 MATa; *his3*Δ1; *leu2*Δ0; *met15*Δ0; *ura3*Δ0; *ire1*Δ::URA *IRE1*-3xHA-yeGFP::HIS pRE375 *IRE1*-3xFLAG-yeGFP::LEU pRE699	This paper
RE726	*IRE1*-3xHA-yeGFP C552 + *CEN IRE1*-3xFLAG-yeGFP C552	BY4741 MATa; *his3*Δ1; *leu2*Δ0; *met15*Δ0; *ura3*Δ0; *ire1*Δ::URA *IRE1*-3xHA-yeGFP::HIS pRE374 *IRE1*-3xFLAG-yeGFP::LEU pRE700	This paper
RE530	*IRE1*-3xHA-yeGFP E540C *single cysteine*	BY4741 MATa; *his3*Δ1; *leu2*Δ0; *met15*Δ0; *ura3*Δ0; *ire1*Δ::URA *IRE1*-3xHA-yeGFP::HIS pRE575	This paper
RE531	*IRE1*-3xHA-yeGFP T541C *single cysteine*	BY4741 MATa; *his3*Δ1; *leu2*Δ0; *met15*Δ0; *ura3*Δ0; *ire1*Δ::URA *IRE1*-3xHA-yeGFP::HIS pRE576	This paper
RE532	*IRE1*-3xHA-yeGFP G542C *single cysteine*	BY4741 MATa; *his3*Δ1; *leu2*Δ0; *met15*Δ0; *ura3*Δ0; *ire1*Δ::URA *IRE1*-3xHA-yeGFP::HIS pRE577	This paper
RE533	*IRE1*-3xHA-yeGFP V543C *single cysteine*	BY4741 MATa; *his3*Δ1; *leu2*Δ0; *met15*Δ0; *ura3*Δ0; *ire1*Δ::URA *IRE1*-3xHA-yeGFP::HIS pRE578	This paper
RE534	*IRE1*-3xHA-yeGFP F544C *single cysteine*	BY4741 MATa; *his3*Δ1; *leu2*Δ0; *met15*Δ0; *ura3*Δ0; *ire1*Δ::URA *IRE1*-3xHA-yeGFP::HIS pRE579	This paper
RE522	*IRE1*-3xHA-yeGFP L545C *single cysteine*	BY4741 MATa; *his3*Δ1; *leu2*Δ0; *met15*Δ0; *ura3*Δ0; *ire1*Δ::URA *IRE1*-3xHA-yeGFP::HIS pRE570	This paper
RE535	*IRE1*-3xHA-yeGFP L546C *single cysteine*	BY4741 MATa; *his3*Δ1; *leu2*Δ0; *met15*Δ0; *ura3*Δ0; *ire1*Δ::URA *IRE1*-3xHA-yeGFP::HIS pRE581	This paper
RE717	*IRE1*-3xHA-yeGFP L547C *single cysteine*	BY4741 MATa; *his3*Δ1; *leu2*Δ0; *met15*Δ0; *ura3*Δ0; *ire1*Δ::URA *IRE1*-3xHA-yeGFP::HIS pRE691	This paper
RE718	*IRE1*-3xHA-yeGFP F548C *single cysteine*	BY4741 MATa; *his3*Δ1; *leu2*Δ0; *met15*Δ0; *ura3*Δ0; *ire1*Δ::URA *IRE1*-3xHA-yeGFP::HIS pRE692	This paper
RE719	*IRE1*-3xHA-yeGFP L549C *single cysteine*	BY4741 MATa; *his3*Δ1; *leu2*Δ0; *met15*Δ0; *ura3*Δ0; *ire1*Δ::URA *IRE1*-3xHA-yeGFP::HIS pRE693	This paper
RE720	*IRE1*-3xHA-yeGFP I550C *single cysteine*	BY4741 MATa; *his3*Δ1; *leu2*Δ0; *met15*Δ0; *ura3*Δ0; *ire1*Δ::URA *IRE1*-3xHA-yeGFP::HIS pRE694	This paper
RE721	*IRE1*-3xHA-yeGFP F551C *single cysteine*	BY4741 MATa; *his3*Δ1; *leu2*Δ0; *met15*Δ0; *ura3*Δ0; *ire1*Δ::URA *IRE1*-3xHA-yeGFP::HIS pRE695	This paper
RE722	*IRE1*-3xHA-yeGFP F544A C552 *single cysteine*	BY4741 MATa; *his3*Δ1; *leu2*Δ0; *met15*Δ0; *ura3*Δ0; *ire1*Δ::URA *IRE1*-3xHA-yeGFP::HIS pRE696	This paper
RE723	*IRE1*-3xHA-yeGFP F531R C552 *single cysteine*	BY4741 MATa; *his3*Δ1; *leu2*Δ0; *met15*Δ0; *ura3*Δ0; *ire1*Δ::URA *IRE1*-3xHA-yeGFP::HIS pRE698	This paper
RE724	*IRE1*-3xHA-yeGFP F531R F544C *single cysteine*	BY4741 MATa; *his3*Δ1; *leu2*Δ0; *met15*Δ0; *ura3*Δ0; *ire1*Δ::URA *IRE1*-3xHA-yeGFP::HIS pRE697	This paper

1088

1089

1090 **Table 2: Plasmids used in this study**

Number	Description	Recombinant DNA	Source
pRE451	*IRE1*-3xHA-yeGFP	pcDNA3.1 *IRE1*-3xHA-yeGFP WT	(25)
pEv200	pRS315 *IRE1*-yeGFP-HA	pRS315 *IRE1*-yeGFP-HA	(28)
pRE375	*IRE1*-3xHA-yeGFP *cysteine-less*	pcDNA3.1 *IRE1*-3xHA-yeGFP *cysteine-less*	This paper
pRE374	*IRE1*-3xHA-yeGFP C552 *single cysteine*	pcDNA3.1 *IRE1*-3xHA-yeGFP C552 *single cysteine*	This paper
pRE699	*CEN IRE1*-3xFLAG-yeGFP *cysteine-less*	pRS315 *IRE1*-3xFLAG-yeGFP *cysteine-less*	This paper
pRE700	*CEN IRE1*-3xFLAG-yeGFP C552 *single cysteine*	pRS315 *IRE1*-3xFLAG-yeGFP C552 *single cysteine*	This paper
pRE575	*IRE1*-3xHA-yeGFP E540C *single cysteine*	pcDNA3.1 *IRE1*-3xHA-yeGFP E540C *single cysteine*	This paper
pRE576	*IRE1*-3xHA-yeGFP T541C *single cysteine*	pcDNA3.1 *IRE1*-3xHA-yeGFP T541C *single cysteine*	This paper
pRE577	*IRE1*-3xHA-yeGFP G542C *single cysteine*	pcDNA3.1 *IRE1*-3xHA-yeGFP G542C *single cysteine*	This paper
pRE578	*IRE1*-3xHA-yeGFP V543C *single cysteine*	pcDNA3.1 *IRE1*-3xHA-yeGFP V543C *single cysteine*	This paper
pRE579	*IRE1*-3xHA-yeGFP F544C *single cysteine*	pcDNA3.1 *IRE1*-3xHA-yeGFP F544C *single cysteine*	This paper
pRE570	*IRE1*-3xHA-yeGFP L545C *single cysteine*	pcDNA3.1 *IRE1*-3xHA-yeGFP L545C *single cysteine*	This paper
pRE581	*IRE1*-3xHA-yeGFP L546C *single cysteine*	pcDNA3.1 *IRE1*-3xHA-yeGFP L546C *single cysteine*	This paper
pRE691	*IRE1*-3xHA-yeGFP L547C *single cysteine*	pcDNA3.1 *IRE1*-3xHA-yeGFP L547C *single cysteine*	This paper
pRE692	*IRE1*-3xHA-yeGFP F548C *single cysteine*	pcDNA3.1 *IRE1*-3xHA-yeGFP F548C *single cysteine*	This paper
pRE693	*IRE1*-3xHA-yeGFP L549C *single cysteine*	pcDNA3.1 *IRE1*-3xHA-yeGFP L549C *single cysteine*	This paper
pRE694	*IRE1*-3xHA-yeGFP I550C *single cysteine*	pcDNA3.1 *IRE1*-3xHA-yeGFP I550C *single cysteine*	This paper
pRE695	*IRE1*-3xHA-yeGFP F551C *single cysteine*	pcDNA3.1 *IRE1*-3xHA-yeGFP F551C *single cysteine*	This paper
pRE696	*IRE1*-3xHA-yeGFP F544A C552 *single cysteine*	pcDNA3.1 *IRE1*-3xHA-yeGFP F544A C552 *single cysteine*	This paper
pRE697	*IRE1*-3xHA-yeGFP F531R F544C *single cysteine*	pcDNA3.1 *IRE1*-3xHA-yeGFP F531R F544C *single cysteine*	This paper
pRE698	*IRE1*-3x-HA-yeGFP F531R C552 *single cysteine*	pcDNA3.1 *IRE1*-3xHA-yeGFP F531R C552 *single cysteine*	This paper

1091